Neuroligin-mediated neurodevelopmental defects are induced by mitochondrial dysfunction and prevented by lutein in *C. elegans*

Silvia Maglioni [1], Alfonso Schiavi [1,6], Marlen Melcher [2], Vanessa Brinkmann [1], Zhongrui Luo [3], Anna Laromaine [3], Nuno Raimundo [4], Joel N Meyer [5], Felix Distelmaier [2], Natascia Ventura [1,6*]

[1] IUF-Leibniz Research Institute for Environmental Medicine, 40225 Duesseldorf, Germany

[2] Department of General Pediatrics, Neonatology and Pediatric Cardiology, University Children's Hospital, Heinrich-Heine-University Düsseldorf, Moorenstr. 5, 40225 Düsseldorf, Germany

[3] Institut de Ciència de Materials de Barcelona, ICMAB-CSIC. Campus UAB. 08193 Bellaterra, Barcelona, Spain.

[4] Department of Cellular and Molecular Physiology, Penn State College of Medicine, 500 University Drive Hershey, PA 17033, United State

[5] Nicholas School of the Environment, Duke University, Durham, NC, United States

[6] Institute for Clinical Chemistry and Laboratory Diagnostic, Medical Faculty of the Heinrich Heine University, 40225 Duesseldorf, Germany

*Corresponding author: natascia.ventura@uni-duesseldorf.de

Abstract

Complex I deficiency represents the most frequent pathogenetic cause of human mitochondriopathies. Therapeutic options for these neurodevelopmental life-threating disorders do not exist, partly due to the scarcity of appropriate model systems to study them. *Caenorhabditis elegans* is a genetically tractable model organism widely used to investigate neuronal pathologies. Here, we generated new *C. elegans* models for mitochondriopathies and showed that depletion of Complex I subunits recapitulates biochemical, cellular and neurodevelopmental aspects of the human diseases. Two models, *nuo-5*/NDUFS1- and *lpd-5*/NDUFS4-depleted animals, were exploited for a suppressor screening that identified lutein for its ability to rescue animals' neurodevelopmental deficits. We uncovered overexpression of synaptic neuroligins as an evolutionarily conserved consequence of mitochondrial dysfunction, which we found to mediate an early cholinergic defect in *C. elegans*. We showed lutein exerts its beneficial effects by restoring neuroligin expression independently from its antioxidant activity, thus pointing to a possible novel pathogenetic target for the human disease.

Abbreviations

ACh, Acetylcholine; *C. elegans*, *Caenorhabditis elegans*; CI, Complex I; DMSO, dimethyl sulfoxide; ETC, mitochondrial electron transport chain; HCS, high-content screening; HMAD, Human Mitochondria-Associated Diseases; HTS, high-throughput screening; NGM, nematode growth medium; NDUFS1, NADH:Ubiquinone Oxidoreductase Core Subunit S1; NDUFS4, NADH:Ubiquinone Oxidoreductase Subunit S4; NMJ, neuromuscular junction; OCR, oxygen consumption rate; ROS, reactive oxygen species; RT, room temperature.

Keywords

C. elegans; Development; Cholinergic synapses; HTS screening; Complex I deficiency; Lutein; Mitochondria diseases; Neuroligin.

Introduction

Over the last few decades, severe mitochondrial dysfunction, most often ascribed to genetic-mediated depletion of mitochondrial electron transport chain (ETC) complex subunits, has been established as the cause of numerous human diseases such as Leigh syndromes, Friedreich's ataxia or Parkinson's disease [1]. In these pathologies the most-affected cells are typically those highly dependent on oxidative energy metabolism such as cardiac and skeletal muscle, pancreatic beta cells and, of course, neurons. Accordingly, mitochondriopathies often present with signs and symptoms that include myopathy, cardiac defects, neuronal abnormalities and sometimes diabetes or additional metabolic dysfunctions. Mitochondrial complex I (NADH:Ubiquinone-Oxidoreductase), the largest of the fours mitochondrial ETC complexes, consists of 44 protein subunits encoded by the nuclear and mitochondrial genomes [2] and it constitutes the main entry point of electrons into the oxidative phosphorylation. Inherited genetic defects leading to human complex I (CI) deficiency are the most frequently encountered defects of the mitochondrial energy metabolism (with an incidence of about 1:8500 living births [3]) and typically cause early-onset neuro-metabolic disorders. Leigh syndrome is a severe disorder ascribed to complex I deficiency, which leads to progressive brain damage and muscular hypotonia [4]. Unfortunately, mitochondriopathies, due to their complexity and variety, are difficult not only to diagnose but also to treat, having very often a fatal outcome, and this is in part due to the scarcity of appropriate model system to study them.

A considerable number of human disease genes have homologs in the genetically tractable model organism *Caenorhabditis elegans*, which has already yielded important insights into disease-relevant molecular mechanisms of many of them [5, 6]. Moreover, *C. elegans'* small size, body transparency, short life cycle and genetic manipulability along with the absence of ethical requirements, make this organism a unique and attractive 3R-compliant model for *in vivo* high-throughput (HTS) screening to search for new therapeutics [7-9]. Several works have indeed already demonstrated the versatility of *C. elegans* in disclosing modifiers of a particular phenotype and their underlying mode of action, and the number of companies that are using *C. elegans* models in the drug discovery process is growing [7]. Notably, *C. elegans* is a powerful model organism for the study of neuronal development and degeneration since 1/3 of its cells are neurons and its nervous system is well characterized both at functional and structural level. Accordingly, the nematode system is successfully used to study neuronal aging and age-associated disease models such as Alzheimer's or Parkinson's diseases [10, 11], and to screen for neuroprotective drugs [12, 13]. Yet, only few studies have exploited *C. elegans* to untangle the pathogenesis and identify possible new treatments for neurodevelopmental pathologies associated with mitochondrial dysfunction and this is at least in part due to the fact that genetic depletion of mitochondrial genes is lethal [14-17]. In this study we therefore specifically followed up on our previous findings revealing a clear threshold effect in determining the opposite - beneficial (e.g. lifespan extension) vs detrimental (e.g. larval arrest) - phenotypes observed upon different degrees of mitochondrial ETC subunit silencing (mild vs severe depletion respectively) [16, 18, 19], to develop novel *C. elegans* models for mitochondriopathies especially linked to severe depletion of CI-subunits.

While not all defects of a complex brain observed in neuronal pathologies can be recapitulated in *C. elegans*, this simple (yet multicellular) model organism may be especially relevant to gain insight into early pathomechanistic consequences of mitochondrial dysfunction overseen in the human diseases, which in most cases present already with overwhelmed and irreversible neurometabolic deficits. Here, we thus exploited *C. elegans* to characterize early biochemical, cellular and neurobehavioral features resulting from severe complex I deficiency. Of note, the discrete and very reproducible phenotypic features resulting from different degrees of mitochondrial dysfunction can be automatically quantified and were therefore utilized for a suppressor screening in search of new potential disease suppressors. We identified lutein, among a small library of natural compounds, for its ability to significantly suppress the arrest

development and neuronal defects we characterized in *nuo-5*/NDUFS1- and *lpd-5*/NDUFS4-depleted animals. Most notably, focusing on NDUFS1, for which there are no other animal models available, we pinpointed lutein protective mechanism through suppression of a neuroligin-dependent cholinergic synaptic defect newly disclosed in the *nuo-5*-depleted animals. Moreover, we confirmed altered expression of synaptic neuroligins in the brain of a NDUFS4 mutated mouse and found that lutein can reduce reactive oxygen species (ROS) production in patients' fibroblasts carrying NDUFS1 or NDUFS4 mutations. Our findings support the validity of exploiting *C. elegans* as a preclinical model to study pathomechanistic aspects of diseases associated with severe mitochondrial dysfunction, in particular with CI-subunit depletion, and most notably point to novel potential targets and therapeutics for the treatment of the corresponding human pathologies.

Results

Development of *C. elegans* models for human mitochondriopathies

To develop new models for mitochondriopathies we silenced a panel of 41 *C. elegans* genes orthologous to nuclear-encoded genes that when mutated in humans lead to severe mitochondrial dysfunction and consequent neurodevelopmental pathologies (**Table 1**; **Table S1**). Two independent rounds of RNAi screen were carried out for two consecutive generations in search of those clones giving the characteristic phenotypic effects associated with different degrees of mitochondrial dysfunction (**Fig 1A; Table 1**) [18, 19]: (i) a "mild" gene suppression causing slight decrease in size and fertility and slow development - phenotypes previously associated with the induction of beneficial pro-longevity mitochondrial stress responses; and (ii) a "strong" gene suppression inducing animals' sterility, growth arrest at the L2/L3 larval stage or lethality, reflecting the deleterious effect ascribed to severe mitochondrial dysfunction. Most of the clones screened showed a "mild" phenotype in the parental generation and a "strong" phenotype in the next generation (**Fig 1B**, P0 vs F1 generations). When a "strong" phenotype was already observed in the parental generation, animals were fed with a diluted dsRNA-expressing bacterial clone to obtain a "mild" phenotype (**Fig 1C**, diluted vs undiluted bacteria). 20 clones (**Table 1**) gave consistent and very reproducible results on animals' development and fertility upon different degrees of silencing and were selected for further characterization (while the remaining 21 clones were not further investigated, **Table S1**).

Interestingly, when lifespan was analyzed, most of the genes, with a few exceptions (e.g. *pdr-1*), still elicited a pro-longevity effect (sometime even greater) when more severely suppressed, although with clear trade-off outcomes on fertility or development as actually expected by a disease state (**Fig S1A; Table S2 and S3**). This implies that, consistent with our recent observation [20], health-related features such as fertility and development reflect the severity of animals' mitochondrial disruption better than lifespan outcomes. Of note, these *C. elegans* detrimental phenotypes are typically associated with severe mitochondrial damage since in this stage mitochondria are necessary in the gonad to start germline expansion and in the nervous system to progress through development [21, 22]. Given their very strong and reproducible phenotype (L2/L3 larval arrest) and health importance in humans (disease prevalence), we then decided to focus on animals with severe suppression of CI-subunits (genes labeled in red in **Table 1**) and further characterized features relevant for the human disorder.

Severe suppression of Complex I subunits impairs neuronal and mitochondrial functionality

Most CI defects are associated with Leigh Syndrome, a devastating neuromuscular degenerative disorder with early childhood onset and very little, and only symptomatic, therapeutic options [4]. Indeed, due to the complexity of the human brain, in most cases the disease already presents with overwhelming neurometabolic abnormalities, which do not allow effective treatment and quickly lead to an inevitable fatal outcome. *C. elegans* gene silencing can be less efficient in neurons. Although animals L3 arrest implies the RNAi is likely working in the nervous system, we first assessed the effect of *nuo-5* and *lpd-5* silencing on development in a neuronal specific sensitive strain and in a strain with overall increased sensitivity to RNAi (but especially in neurons). Interestingly, the effect of the RNAi was reduced in the first strain while it was increased in the second one (**Fig S1B**), indicating that systemic mitochondrial suppression has broader repercussion than neuronal silencing. Thus, to closely recapitulate the systemic mitochondrial disease state and avoid possible confounds due to strains genetic background, we decided to continue our characterization using systemic RNAi in the wild-type *C. elegans* strain.

Most notably, we exploited the power of nematode behaviors to reveal possible early neuromuscular functional deficits induced by mitochondrial deficiency. Using different chemicals, which in *C. elegans* are sensed by different sub-classes of neurons, we assessed animals chemotaxis in L3 larvae, a very sensitive readout of animal health [23] and found that

strong suppression of the different CI subunits caused a significant neuronal impairment compared to stage-matched controls (**Fig 2A,B; Fig S2A-D; Table S4**). Besides the neurodevelopmental defects CI-deficiency typically manifests with rapid deterioration of the motor function. Interestingly, severe suppression of different CI-subunits did not significantly reduced animals' ability to move in solid agar plate compared to wild-type animals (**Fig S2E**), with the exception of one clone, *nuo-1*. Yet, notably, similar to the perceived fatigue often observed in patients with mitochondrial disorders [24], a locomotion defect could be revealed under energetic challenge, a condition that in *C. elegans* can be simulated by swimming [25] (**Fig S2F**).

For further characterization of our models, we then narrowed our study to two CI subunits, namely LPD-5 (NDUFS4 homolog), an 18-kDa subunit predicted to have oxidoreductase activity and NUO-5 (NDUFS1 homolog), a 75-kDa subunit thought to be the first of many Fe-S proteins to accept electrons from an NADH-flavoprotein reductase. Both subunits are part of the CI functional N-module, the structure responsible for oxidation of NAD(P)H to NAD^+. NDUFS1 is one of the so-called core subunits, which are conserved from bacteria to human, while NDUFS4 is one of the accessory subunits, which have been shown to vary between species [26]. NDUFS1 is essential for the enzymatic function, specifically for the electron transfer within CI [27] while NDUFS4 seems to be crucial for the assembly and stability of the complex [28]. Since cardiopulmonary failure is most often the underlying cause of mortality in patients with mitochondrial disorders, we characterized animals pharyngeal muscle functionality. Indeed, similarities between *C. elegans* pharyngeal muscle and the vertebrate heart in terms of anatomic development and physiology have been described, which suggest convergent evolution between two autonomous muscular pumps with similar biological roles [29]. Strikingly, automatic measurement through a microfluidic device [30] revealed that *nuo-5* and *lpd-5* RNAi-treated animals have an abnormal electropharyngeogram (EPG) with significantly decreased pump frequency (**Fig 2C**) and increased average inter-pump interval (IPI) as well as R o E ratio when compared to control nematodes (**Fig S2G,H**).

Mitochondrial respiration was then also measured with the Seahorse Bioscience Flux Analyzer, optimized for nematodes at L2/L3 larval stage [20]. Consistent with a mitochondrial disease state, most parameters associated with mitochondrial respiration were significantly affected upon severe suppression of *nuo-5* or *lpd-5* compared to wild-type animals. Specifically, basal oxygen consumption rate (OCR), maximal respiratory capacity (upon treatment with the uncoupling

agent carbonyl cyanide 4-trifluoromethoxy-phenylhydrazone), ATP-linked OCR (in the presence of the ATP inhibitor Dicyclohexylcarbodiimide) as well as steady-state ATP levels, were halved compared to control animals (**Fig 2D-G**). Spare respiratory capacity (resulting by subtracting basal from maximal OCR), which indicates organism's ability to respond to increased energy demand, and proton leak, were however only significantly reduced in *nuo-5*-depleted animals (**Fig S3A,B)**. Interestingly, *nuo-5* and *lpd-5* RNAi as expected significantly increased reactive oxygen species (ROS) production (**Fig 2H**), but did not induce any major sign of oxidative damage at least at this early stage: the expression of a classical oxidative stress sensor (p38MAPK/*pmk-1*) was not affected (**Fig S3C**) and actually both lipid and amide oxidation were diminished (**Fig S3D,E**). Moreover, although mitochondrial DNA is especially sensitive to oxidative damage [31], *nuo-5* and *lpd-5* RNAi-depleted animals only presented with nuclear but not mitochondrial DNA damage (**Fig S3F,G**) and, quantitative measurements of mitochondrial genome copy number, which can be oxidative stress-responsive [32], also did not reveal any significant difference between control and RNAi-treated animals (**Fig S3H**). These results suggest the induction of stress response defensive mechanisms. Accordingly, *nuo-5* and *lpd-5* RNAi increased the expression of genes involved in mitochondrial quality control pathways [16, 33]: the antioxidant response gene glutathione-S-transferase *gst-4*, the mitochondrial unfolded protein response gene *hsp-6*, and the mitophagy regulator Bnip3 homolog *dct-1* (**Fig 2I-K; Fig S4A**). Disturbing *C. elegans* mitochondrial function also induces autophagy, lipid remodeling [34] as well as drug detoxification and pathogen-response genes [35]. The nuclear translocation of HLH-30, a common regulator of these 'cytoprotective' pathways [36], was also significantly increased in *nuo-5* and *lpd-5* arrested L3 animals (**Fig 2L; Fig S4B**), differently from pro-longevity *daf-2* RNAi that only promoted HLH-30 activation in adults but not in the L3 larvae (**Fig S4C**). This indicates that differently from the beneficial activation of TFEB/HLH-30 induced by DAF-2 suppression [36], activation of this transcription factor early in life is rather associated with detrimental effects. Taken together, characterization of our new models indicates that, similar to the human disease, animals with CI-subunits depletion display severe mitochondrial, cellular, developmental and neuromuscular defects.

A phenotype-based screening identifies Lutein as a Complex I disease suppressor

In vivo genetic and compounds screening with model organisms exponentially grew in the past decade as strategies to identify modifiers of specific phenotypes ranging from simple proteins

expression to more complex animals' behaviors such as aging or disease-associated features [5, 7, 37]. Nutraceuticals supplemented through the diet may provide more feasible therapeutic opportunities than genetic or pharmacological interventions. We thus specifically took advantage of the reproducible, discrete and automatically quantifiable disease-relevant phenotype – developmental arrest – observed upon severe mitochondrial dysfunction, to screen a small library of mainly natural compounds in search of potential disease suppressors. The developmental arrest induced by severe knock down of CI proteins might however be irreversible or require a treatment at a specific stage in order to be prevented or rescued. Thus, we first used two different approaches to have a proof of principle of the feasibility of our suppressor screen. In the first approach we took advantage of the p53 *C. elegans* mutant, *cep-1(lg12501)*, which can prevent the developmental arrest induced by severe suppression of *nuo-2* and of other mitochondrial proteins [19]. Lack of *cep-1* also partially rescued the development arrest observed in different disease models (**Table S5**), indicating the arrest is reversible. In the second approach, we moved the F1 progeny from RNAi-expressing- to empty vector-expressing- bacteria at different stages, namely from eggs to L3. Depending on the disease model, the developmental arrest could be prevented moving the animals on control bacteria from eggs to L2, but in most cases not after L3 arrest (**Fig S5A; Table S5**), with obvious implications for the efficacy of a possible therapeutic approach.

A total of 37 compounds were then supplemented at different concentrations (ranging from 0.5 µM to 1 mM) to the second generation of animals (starting from eggs) fed UVB-killed bacteria transformed with either control vector or with *nuo-5* or *lpd-5* dsRNA (**Fig S5B**). Among tested conditions (compounds & doses), 11 partially prevented the developmental arrest induced by *nuo-5* RNAi, while 7 rescued that of *lpd-5* RNAi, resulting in a total of 12 compounds, which allowed more than 20% of worms to develop into fertile adults after 6 days of treatment (**Fig 3A-C; Fig S6A,B; Table S6**), compared to wild-type animals which developed into adults in 3 days. Significant differences were achieved only with isovitexin 10µM on *nuo-5*, with kahalalide F 0,5µM on *lpd-5* and with lutein 1µM on both. Moreover, out of twelve compounds only three, i.e. lutein, isovitaxin and macrosporin, were effective against both RNAi (**Fig 3A-C**). We then looked at the effect of these three on development from day 4 to 6 and observed that the effect of lutein was the most reproducible and significant (**Fig S7A-C**).

To avoid misleading interpretation of compounds effects we then excluded that most relevant compounds did not generically (i.e. *skn-1* or *phi-7* RNAi-induced embryonic lethality, **Fig**

S7D,E) or specifically (i.e. *nuo-5* transcript expression, **Fig 3D**) affect the efficacy of the RNAi. Finally, since energetic defects upon *nuo-5* and *lpd-5* depletion may impact on compounds absorption and/or metabolism measured lutein accumulation inside the animals. Importantly, through infrared micro-spectroscopy we could detect lutein absorbance peak at 1515.8 cm^{-1} [38] in the worms (**Fig 3E**), confirming that animals uptake the drug independently of the mitochondrial deficiency. We thus identified lutein as a nutraceutical able to significantly and specifically prevent the developmental arrest induced by systemic mitochondrial deficiency.

Lutein is a carotenoid belonging to the xanthophyll family that is found abundantly in leafy dark green vegetables, egg yolk, animal fat and human eye retinal macula [39]. Increasing evidence points towards the beneficial effects of lutein in several pathological conditions, ranging from cancer to neurodegenerative disorders [40-42]. Strikingly, we found that lutein not only partially rescued the developmental defect of *nuo-5* or *lpd-5* depleted animals (**Fig 3C**), but also significantly ameliorated their neuronal deficits (**Fig 3F-I**). Specifically, lutein fully suppressed the chemotaxis defect induced by *nuo-5* and *lpd-5* RNAi towards different chemicals, in some cases even above the level of wild-type lutein-treated animals. Indeed, lutein enhanced the sensory neuron functionality in the wild type animals, but this improvement was greatly accentuated in the *nuo-5* and *lpd-5* depleted animals (**Fig 3F-I**). Importantly, lutein also suppressed the pharyngeal pumping defect observed in the disease models (**Fig 3J; Fig S7F**).

The most likely physiological functions of this pigment are protection against oxidative- and radiation- induced damage of membrane's lipids [43]. Accordingly, lutein was able to decrease ROS in *nuo-5*- and *lpd-5* depleted worms (**Fig 3K**) and completely prevented *hlh-30* activation (**Fig 3L**), which may indeed be increased either by ROS or mitochondrial damage. Of note, lutein also decreased ROS levels in fibroblasts derived from patients carrying mutations in the corresponding human homologs NDUFS1/*nuo-5* and NDUFS4/*lpd-5* (**Fig 3M; Fig S8A,B**). However, while *nuo-5* and *lpd-5* depleted animals were more sensitive to the mitochondria ETC inhibitor sodium azide, lutein failed to protect against it (**Fig S8C**), it did not consistently suppress the induction of mitochondrial stress response genes (**Fig S8D-G**) and it did not modulate oxidation of cellular components (**Fig S8H-I**). Moreover, we tested the effect of other antioxidants with known effect on another *C. elegans* model for Complex I disease [15], namely N-Acetyl-cysteine (NAC), Vitamin C (VitC) and Coenzyme Q10(CoQ10) and found that while general antioxidants such as NAC and vitC, similar to lutein, prevented the developmental arrest *nuo-5* depleted animals, this was not the case with the mitochondrial antioxidant coQ10 (**Fig**

S8J). Taken together, results described so far revealed that lutein substantially ameliorates developmental, neuronal and cellular dysfunction upon depletion of CI subunits but most likely impinging on downstream mitochondrial-modulated processes rather than through direct beneficial effects on mitochondria.

Lutein rescues a newly identified synaptic defect in NDUFS1/*nuo-5*-depleted animals

To gain insight into the molecular mechanisms accounting for the deleterious outcomes induced by severe mitochondrial dysfunction and the protective effects of lutein, we (i) first compared the transcriptomic profile of stage-matched (L3 larvae) cohorts of wild-type animals with that of larvae subjected to mild or strong *nuo-5* RNAi (**Fig 4A**); (ii) and then compared the transcriptomic profile of strong *nuo-5* RNAi animals, treated and untreated with lutein, with that of animals fed empty vector control. Remarkably, mild mitochondrial stress led to very few changes in gene expression in the L3, in stark contrast with differences observed in the adults [44, 45]. Only four genes, *fmo-2, B0205.13, T16G1.6 and nuo-5,* were indeed differentially expressed between control and mild *nuo-5* RNAi, based on a relatively liberal FDR-corrected $p < 0.05$ cut-off, with *nuo-5* expression being more severely suppressed upon strong RNAi. Moreover, consistent with the different degree of mitochondrial disruption [20], the 303 genes differentially expressed uniquely between mild and severe *nuo-5* treatments all belong to GO terms associated with mitochondria (**Fig 4B,D,F**), clearly indicating that the metabolic alterations we previously observed in response to mild mitochondrial stress [20] precede genomic reprogramming. Thus at least at this early developmental stage, the mitochondrial remodeling upon mild mitochondrial stress appears to successfully compensate for the genetic deficiency, obviating the need for detectable transcriptional changes. In contrast, large transcriptomic changes are triggered in larvae upon severe mitochondrial stress. Interestingly, the 1152 genes uniquely different between control and strong *nuo-5* suppression, revealed GO terms affecting multiple cellular compartments (**Fig 4C,E,G**), from nucleus to cytoplasm to the Golgi apparatus and membrane components, as well as genes involved in lifespan determination, ribonucleoprotein complex biogenesis and neuropeptide signaling, thus displaying a more general cellular remodeling not only limited to mitochondria.

Accordingly, in the second transcriptomic analysis, the comparison between wild-type and strong *nuo-5* depleted animals revealed 2274 altered genes (**Fig 5A**), implicated in fundamental cellular morphogenesis processes and especially, as expected, in organismal and nervous system

development (**Fig S9A; Table S7**), reflecting the very strong effect of the treatment on worm's biology ultimately leading to growth arrest. On the other hand, interestingly, when comparing wild-type animals with *nuo-5* treated with lutein (rescued animals), the number of altered genes diminished to 1296, indicating that roughly half of the genes were restored to wild-type levels. Notably, consistent with the rescue of the neurodevelopmental deficits observed upon lutein treatment, most of these genes belong to developmental and neuronal processes (**Fig S9B; Table S7**). We then focused our attention on the differences between *nuo-5* depleted worms left untreated or treated with lutein, and identified 143 differentially expressed genes (**Fig 5A,B; Table S8**). Analysis of *nuo-5* expression in the microarray data supported previous qPCR results and confirmed that lutein-rescuing effects are specific and not ascribed to a reduced potency of the *nuo-5* RNAi (**Fig 5C**). Moreover, the heatmap (**Fig 5B; Table S8**) and the analysis of a sample of genes (**Fig 5D-F**) demonstrated the high reproducibility of the data. Intriguingly, GO analysis of (**Table S7**) revealed four main molecular pathways enriched upon lutein treatment in *nuo-5* depleted animals: (i) secretion (synaptic and neurotransmission regulation), (ii) endosomal transport, (iii) protein import into the nucleus and (iv) mitotic sister chromatin segregation (cell cycle) (**Fig 5G**). In support of the cellular defects, no major signature relative to oxidative stress responses or damage were revealed in this early developmental stage. Instead, we speculated that defective mitochondria-induced energetic failure negatively impacts on vesicle trafficking and consequently synaptic functionality, which is somehow rescued by lutein.

To address our hypothesis, we took advantage of behavioral assays commonly used to assess synaptic functionality in *C. elegans* [46-50]. Synaptic transmission mutants display altered resistance to aldicarb, an acetyl-cholinesterase inhibitor [47]: mutants with increased cholinergic transmission are hypersensitive to aldicarb and paralyze faster than wild-type animals (Hic phenotype), while mutants with reduced cholinergic transmission have increased resistance and take longer time to paralyze upon aldicarb treatment (Ric phenotype). Strikingly, in support of our hypothesis, *nuo-5* depleted larvae paralyzed faster than stage-matched wild-type in the presence of the same concentration of aldicarb, indicating an increased cholinergic transmission. Most notably, *nuo-5* worms treated with lutein from eggs to L3 larvae lose the Hic phenotype and have a normal response to Aldicarb (**Fig 6A**). The Hic phenotypes could be ascribed either to pre-synaptic alterations, such as inability to negatively regulate pre-synaptic ACh release or reuptake, or to post-synaptic defects, like loss of post-synaptic ACh regulation or inhibitory GABA transmission. Since the aldicarb assay does not distinguish between these different

scenarios we took advantage of levamisole, a selective agonist of the nicotinic acetylcholine receptors found at the postsynaptic side of the neuromuscular junction (NMJ) [48]. Wild-type nematodes exposed to levamisole paralyze over time due to excessive excitation of the acetylcholine receptors and worms with loss of function mutations in these receptors are usually more resistant to levamisole. Instead, animals with mutations affecting presynaptic function paralyze either to a similar speed or slightly faster than wild-type on levamisole plates (due to a possible compensatory postsynaptic increase in cholinergic receptors expression or function) [51, 52]. We observed that *nuo-5* deficient worms also paralyzed faster than wild-type animals in response to levamisole (**Fig 6B**), which is still compatible with exaggerated pre- or post-synaptic activity. This paralysis was however not significantly reverted by lutein pointing towards its protective effect at the presynaptic rather than post-synaptic level or in the synaptic cleft.

The partial effect of lutein on levamisole-induced paralysis could be due to an excessive levamisole concentration and/or activation of postsynaptic receptor compensatory mechanisms or to a concomitant defect in the GABA inhibitory system. To discriminate between these different possibilities, we took advantage of a complementary assay, which exploits pentylenetetrazole (PTZ) [49], a GABA receptor antagonist. In response to PTZ, neurotransmission mutants display different phenotypes: wild-type worms and mutants with defects in ACh release do not display PTZ sensitivity, due to appropriate regulation of ACh amount and activity; mutants that cannot negatively regulate ACh release, and thus secrete excessive amounts of ACh become completely paralyzed upon PTZ treatment [49]; GABA receptors mutants (e.g. *unc-49*) instead, only display dose-dependent paralysis of the body (but not of the head) resulting in head convulsions (head bobs). We found that *nuo-5* depleted worms responded to PTZ with a significantly higher percentage of full-body paralysis, and only a small non-significant fraction of head convulsions; most importantly, lutein treatment significantly suppressed the full body paralysis but not the head convulsions (**Fig 6C**). Overall, our paralysis assays: lead to the identification of a pre-synaptic defect induced by severe mitochondrial deficiency; are specifically consistent with the inability to negatively regulate ACh release, while excluding a major defect in GABAergic transmission [50]; indicate a rescuing effect of lutein on the altered negative feedback on ACh release (**Table S9**).

Synaptic neuroligin expression is increased upon CI deficiency and suppressed by lutein

We then turned to our microarray results to identify possible pathogenetic target of lutein. We confirmed the effect of lutein on some *nuo-5* RNAi-induced genes, such as *vps-35*, *nlp-40* and *unc-10* (**Fig S10A**), highly representative of the two main GO categories (**Fig 5C**). We also exploited GFP reporter strains to analyze the expression of different genes specifically involved in synaptic functionality: the expression of *unc-10*, involved in synaptic membrane exocytosis [53], was significantly induced by *nuo-5* RNAi and suppressed by lutein; the expression of *glb-10*, required for synaptic structure and function [54], was reduced by *nuo-5* RNAi and returned to levels similar to control upon lutein treatment; *unc-17*, a gene required in cholinergic neurons to load acetylcholine into synaptic vesicles [55], was increased by *nuo-5* RNAi and reduced to control levels upon lutein treatment (**Fig 6D-F; Fig S10B-D**). Moreover, we plotted the expression of genes involved in synaptic vesicle cycle from the microarray and found them to be all significantly altered in *nuo-5* animals compared to control (**Fig 6G**). However, when we compared the expression of these genes in *nuo-5* vs *nuo-5* treated with lutein, the only significantly altered transcript was *nlg-1* (**Fig 6H**). NLG-1 is a presynaptic cell adhesion protein, neuroligin, which along with postsynaptic neurexin (NRX-1), mediates in *C. elegans* a retrograde signal that inhibits neurotransmitter release at NMJ [56]. Remarkably, we found a conserved and consistent upregulation of different neuroligin (NLGN1-2 and 4) and neurexin (NRX1 and 3) genes in the brain of NDUFS4 KO mice compared to wild-type animals (**Fig 7A; Fig S10E-F**). Closer analysis of *nlg-1* interactors from the microarray revealed the expression of two of them (*madd-4* and *dlg-1*) to be significantly changed by *nuo-5* RNAi compared to control and, although not in a significant manner, to be altered upon lutein treatment (**Fig 7B-C**). Using a *C. elegans* transgenic reporter strain to quantify the expression of *nlg-1*, we confirmed a significant increase in *nuo-5* depleted animals which went back to wild-type levels upon lutein treatment (**Fig 7D-E**). These observations along with the altered behavioral assays, are indicative of an excessive buildup of Ach in the synaptic cleft in the disease model, a defect that is considerably rescued by lutein.

Up-regulation of *nlg-1* is required in *C. elegans* to enhance synapses strength and prevent neuronal degeneration in response to oxidative stress [57]. Thus, to assess whether lutein reduced *nlg-1* expression and rescue synaptic functionality possibly through its antioxidant activity we tested the effect of above-mentioned antioxidants in *nuo-5* depleted animals on aldicarb-induced paralysis and *nlg-1* expression. Very interestingly, within different antioxidants, NAC was the

only one capable of suppressing aldicarb sensitivity to a similar extent than lutein (**Fig 7F**), but contrary to lutein it did not rescue *nlg-1* overexpression (**Fig 7G**). These data are in agreement with our cellular and transcriptomic analysis and suggest that lutein may exert its beneficial effect at synapsis independently of its antioxidant activity.

Neuroligin mediates the protective effect of lutein on cholinergic synapses

We then reasoned that *nlg-1* is increased in *nuo-5*-depleted animals to compensate for a mitochondrial-stress-induced synaptic defect, and its downregulation upon lutein treatment likely represents a consequence of its beneficial effects on specific mitochondria-regulated neuronal functions. In this scenario knock-out of *nlg-1* should worsen the deleterious effects of *nuo-5* RNAi and lutein may still retain some beneficial effects. Interestingly, contrary to our expectation *nlg-1* knockout per se significantly ameliorated neuromuscular (trashing, sensitivity to aldicarb and levamisole, as well as full body paralysis in response to PTZ**, Fig 8A-D; Fig S11A-G**) induced by *nuo-5* silencing, without any obvious alteration in control animals. Strikingly, a similar protective effect of *nlg-1* knockout was observed against *nuo-5*-induced developmental defects in two different *nlg-1* knock-out alleles, thus excluding unspecific effects due to animals' genetic background (**Fig 8E; Fig S12A**). These results imply that induction of *nlg-1*, contrary to the protective effect that has been observed against acute oxidative stress [57], has instead a detrimental effect when upregulated in response to chronic and severe mitochondrial dysfunction. In strong support of a beneficial effect for *nlg-1* suppression, the *nlg-1* knockout strain also clearly masked the beneficial effects of lutein in mitochondria defective animals (**Fig 8A-E; Fig S11A-G**).

Of note, in further support of a detrimental effect ascribed to *nlg-1* overexpression upon CI deficiency, two strains overexpressing NLG-1, namely a translational reporter P*nlg-1*::NLG-1::GFP [57] and a *nlg-1*(ok259) knockout strain rescued by a P*nlg-1*::NLG-1 array [58], displayed already severe neurodevelopmental phenotypes when grown on *nuo-5* or *lpd-5* RNAi in the parental generation. Specifically, when the transgenic P*nlg-1*::NLG-1::GFP was fed *nuo-5* or *lpd-5* RNAi we could already observe an increased expression of *nlg-1* in the parental generation (**Fig 8F**), which became sterile. Accordingly, also the *nlg-1*(*ok259*) rescued strain became sterile upon mitochondrial deficiency already in the first generation (**Fig S12A**). Most importantly, NLG-1 rescue restored the beneficial effect of lutein in the aldicarb sensitivity assay to the degree of the wild-type animals (**Fig 8G**) confirming lutein works through suppression of

nlg-1. Overall, we revealed for the first time a pathogenetic role for *nlg-1* overexpression upon mitochondrial dysfunction, which mediates an altered synaptic functionality restored by lutein, thus pointing towards a novel potential targeted therapeutic for the corresponding human pathologies.

Discussion

In the present work, we developed and thoroughly characterized new *C. elegans* models for mitochondriopathies, and focused on CI-deficiency associated to NDUFS1/*nuo-5* and NDUFS4/*lpd-5* depletion to carry out a phenotype-based screening in search of disease suppressors. We identified a nutraceutical, lutein, which significantly prevented the neurodevelopmental deficits observed in the two disease models. Importantly, we found that lutein exerts its beneficial effect by rescuing a synaptic defect, which we described for the first time in NDUFS1/*nuo-5* depleted animals. We specifically identified overexpression of the *C. elegans* neuroligin homolog, *nlg-1*, as a novel mediator of the developmental and synaptic defects observed upon severe mitochondrial dysfunction and suppressed by lutein (**Table S9**) which, based on the conserved overexpression in mice, may represents a new relevant pathogenetic and therapeutic target for the human disease.

To date, experimental animal models for CI disorders are scarce (e.g. Ndufs4 mutant mice) [59], do not fully recapitulate the disease state (e.g. Surf1 mutant mice) [60] or do not exist (e.g. Ndufs1) thus seriously hampering the development of adequate therapeutic strategies, which indeed are not available for these devastating disorders with fatal outcome. As a consequence, studies revolved at investigating CI disorders and potential therapeutic strategies are primarily carried out in patients' fibroblasts or lymphoblasts, which, although certainly useful, are not the most relevant systems to recapitulate diseases of the nervous system [2].To overcome cell-specific limitation, more recent and exponentially growing approaches (including our ongoing studies) rely on iPS-derived neuronal systems [61]. Although very promising, these structures lack the complexity of the whole organism thus potentially precluding identification of important cell-non-autonomous effects induced by mitochondrial dysfunction, which may have important implication for disease development, progression and therapy. This is supported by our data in the neuronal specific and hypersensitive RNAi backgrounds clearly indicating systemic mitochondrial suppression has stronger and broader repercussion than neuronal silencing.

Therefore, in the first part of this work, to generate new animal models for mitochondriopathies, we carried out a customized RNAi screen against genes whose severe deficiency in human is associated with mitochondrial disorders. We identified for half of the clones under study a dose-dependent response to the gene silencing, which mimics the disease progression and is consistent with the mitochondrial threshold effect. Namely, compensatory metabolic reprogramming and signaling pathways may help coping with a mild mitochondrial stress, yet, after a certain threshold of mitochondrial dysfunction is reached, these processes are no longer protective and detrimental features arise, such as mitochondrial and neurodevelopmental deficits [6, 16, 18, 20]. Very interestingly, we found that animals with mild and severe mitochondrial disruption were in most cases equally long-lived compared to wild-type, indicating that signaling pathways specifying development and lifespan upon mitochondrial stress are uncoupled. Consistent with this scenario, the gene expression profiles in the L3 larvae indicated that remodeling of mitochondrial structure and function underlies the main (developmental) differences observed between mild and strong *nuo-5* suppression. Yet, changes in lifespan-regulatory pathways normally observed in adult upon pro-longevity mitochondrial stress [44, 45] are not observed in the L3, while are already visible upon severe mitochondrial suppression. Along with the respiration profiles, these data support previous works indicating that mitochondrial changes are not all relevant for longevity specification but rather correlate with developmental outcomes [20, 62, 63].

Regardless of lifespan specification, we showed that about 50% reduction in *nuo-5* transcript expression is clearly sufficient to significantly reduce neurometabolic parameters (around 50%) and to induce changes in the expression profile of mitochondrial and metabolic genes, which are very similar to the mitochondrial deficits [2] and the proteomic changes [27] observed in Ndufs1 patients' fibroblasts. Severe suppression of different mitochondrial diseases-associated genes induced very reproducible *C. elegans* phenotypes (developmental arrest or reduced body size), which were essential to carry out our suppressor screen. Yet, consistent with the heterogeneity of signs and symptoms of these mitochondrial disorders [27, 64], we also observed variability in the extent of different phenotypic outcomes e.g. locomotion and chemosensory deficits, mitochondrial respiratory parameters, ability of compounds to rescue the developmental arrest. We initially assumed the movement defect simply arises at a later age, as previously described [23], but we could actually uncover it under increased energetic request. Interestingly, this behavior is similar to the perceived fatigue often observed in patients with

mitochondrial disorders [24] and given the suppressive effect of lutein, it provides us with a very sensitive and quick assay for future suppressor screening. It will be very important to further investigate whether depletion of other CI subunits or of other mitochondriopathies associated genes increases sensitivity to metabolic or environmental/dietary stressors as these factors may influence mitochondrial activity and have devastating consequence in patients [65, 66]. Interestingly, we also found a defect in animals' pharyngeal pumping, a very relevant phenotype considering the similarities between *C. elegans* pharynx and the human heart, and the fact that patients with mitochondrial disorders often present with, and die for, cardiac dysfunction.

At the cellular level, we observed increased ROS production in both *C. elegans* and patients' fibroblasts, accompanied by increased expression of mitochondrial stress response genes (i.e. *gst-4, hlh-30*, *dct-1*, and *hsp-6*) and increased sensitivity to oxidative stress in *nuo-5*- and *lpd-5* depleted animals. Yet, at least at this early stage we have looked at, oxidative stress and damage do not seem to play a major role in eliciting or suppressing animals' phenotypes. In fact, proton leak as well as lipid and amide oxidation were actually reduced and a classical oxidative stress response gene (p38MAPK/*pmk-1*) was not activated in the disease models. Furthermore, while lutein significantly suppressed neurodevelopmental deficits, as well as the induction of *hlh-30* in the two disease models, it neither suppressed the induction of *gst-4* or *hsp-6* nor modulated animals' sensitivity to oxidative stress. Interestingly, *dct-1* expression was regulated in opposite direction by lutein in the two disease models, perhaps indicating that an optimal level of mitophagy must be achieved for proper mitochondria turnover. Thus, *hlh-30*/TFEB-regulated autophagy and *dct-1*/Bnip3-regulated mitophagy may represent protective mechanisms against the mitochondrial defects or may induce deleterious effects if over-activated in the disease. Regardless, fine-tuning of these processes, which have been already implicated in the pathogenesis of different neuromuscular disorders, may be seen as part of a cytoprotective effect promoted by lutein. Remarkably, through a combination of genetic and behavioral assays we were able to uncover for the first time an acetylcholine presynaptic alteration upon severe mitochondrial dysfunction (most likely an impairment in the ability to negatively regulate ACh release at the NMJ), which was prevented by lutein treatment. Of note, both mitochondria and autophagy play critical role in shaping synaptic structure and function [67, 68] and our microarray data pointed towards genes regulating neurotransmitter secretion and endosomal transport as two out of four main pathways affected by lutein in the disease model. It will be thus very interesting to untangle how CI deficiency provokes synaptic alteration and whether

autophagy and/or mitophagy, which we found to mediate mild mitochondrial stress extension of lifespan [34, 69], also play a role in this pathological context.

Intriguingly, we showed that within different synaptic regulatory genes affected by *nuo-5* depletion, lutein treatment consistently and significantly abolished the upregulation of neuroligin (*nlg-1*), a cell adhesion synaptic protein that along with its partner protein neurexin, mediate a retrograde synaptic signaling that inhibits neurotransmitter release [56, 58]. Interestingly, abnormal expression of extracellular adhesion molecules has been observed in Ndufs1 fibroblast [27], yet, not surprisingly, we could not find any specific change in neuroligin expression in the ndufs1/4 fibroblasts (*not shown*). Instead, most importantly, we found different neuroligins and neurexin genes also significantly upregulated in the brain of *Ndufs4* knockout mice, suggesting abnormal synaptic neuroligin expression as common pathogenetic denominator of different CI-linked disorders. In support of a detrimental effect of neuroligin overexpression, *nlg-1* knockout rescued the neuronal deficits and, strikingly, also partially the developmental defect, induced by mitochondrial dysfunction, masking the beneficial effects of lutein. This is opposite to the protective role previously described in *C. elegans* neurons, where induction of *nlg-1* by *skn-1/*Nrf2 (which is activated by lutein in mammals [70]) confers resistance against acute oxidative stress [57]. Our data clearly suggest *nlg-1* may play opposite effects depending on the context and imply lutein suppresses its expression likely through ROS-independent mechanisms modulated downstream to mitochondria. Accordingly, although *nuo-5* and *lpd-5* depleted animals were more sensitive to oxidative stress, lutein neither affected this response, nor suppressed *nuo-5* RNAi-induction of *gst-4* (a well-established *skn-1* target in response to oxidative stress) or of other mitochondrial stress response genes. In support of ROS-independent regulation of *nlg-1* in this context, whilst interrogating the effects of different antioxidants known to rescue deleterious phenotypes in other CI disease models (i.e. NAC, VitC and CoQ10 [15]), we found that only NAC improves the synaptic functionality of *nuo-5* depleted animals yet without suppressing *nlg-1* overexpression. It will be interesting to further investigate how abnormal expression of neuroligin impacts on animals' neuronal function and development in response to mitochondrial deficiency.

Mitochondria regulate synaptic activity in many ways and severe mitochondrial dysfunction is therefore expected to have broader repercussion on synaptic regulatory proteins [67]. Increased expression of NLG-1 may thus represent a neuronal attempt to compensate for compromised synaptic signaling induced by the mitochondrial deficiency. However, rather than

protective, this would lead to a pathological synaptic excitation, which, as supported by our transcriptomic and behavioral (aldicarb, levamisole and PTZ sensitivity) data, was in fact rescued by lutein suppression of NLG-1. Chronic exposure to lutein in the diseased worms could thus activate NLG-1-regulated compensatory mechanisms that rescued their paralysis defects. Interestingly, NLG-1 contains an extracellular cholinesterase-like domain that forms the interaction with the neurexin domain [71], and lutein was shown to have acetylcholinesterase (AChE) inhibitory activity [72]. Whether lutein neuroprotection upon CI deficiency is mediated by direct inhibition of synaptic AChE and/or NLG-1 activity (in turn suppressing compensatory *nlg-1* overexpression), is an attractive possibility that requires further investigation. It is worth noting that Alzheimer's disease (AD) patients were reported to have significantly less macular pigments (comprising lutein, zeaxanthin and meso-zeaxanthin) and lower serum concentrations of lutein and zeaxanthin compared to control subjects [73] and that AChE inhibitors are the standard therapy for AD [74]. Moreover lutein was shown to have beneficial effects in AD patients [42] (who interestingly also display neuroligin-mediated synaptic dysfunction [75]), as well as against other neuropathological conditions such as diabetic retinopathy [76], age-related macular degeneration [41], and Parkinson disease [77], primarily due to its antioxidant, anti-apoptotic and mitochondrial protective properties. We provide for the first time the proof of principle for considering lutein as a new and easily accessible therapeutic for mitochondrial diseases associated with CI deficiency, which to date present with no cure. Lutein can be naturally ingested either through the diet (dark leave vegetables) or as a dietary supplement or as an ingredient in nutraceutical foods. However, due to its highly hydrophobic nature different strategies are being developed to improve its bioavailability [72, 78, 79], which can therefore offer more effective therapeutic strategies. Finally, besides lutein, our suppressor screen identified few other compounds that partially rescued the developmental arrest of CI deficient animals and it will be interesting to assess them alone or in combination with lutein in the different neuronal assays.

In summary, in this work we established new *C. elegans* models for devastating neurodevelopmental disorders, which to date present with no cure, and focused our attention on the CI deficiency model associated with NDUFS1 depletion, to our knowledge the first and only animal model available for this disease. This simple (yet multicellular) model organism, with its reduced nervous system complexity and powerful neurobehaviors represents a great opportunity to identify early pathomechanistics defects causally involved in the disease. Our results support

the growing body of evidence indicating that live animal screens are ideal tools for drug discovery strategies designed to identify suppressors of specific and complex disease-associated phenotypes [80-82]. Most importantly, although validation in mammalian systems is required to encourage translational studies, we provided the rationale for suggesting lutein as a novel therapeutic to rescue a neuroligin-mediated synaptic dysfunction disclosed for the first time upon CI-deficiency.

Materials and Methods

C. elegans methods

C. elegans strains and maintenance

We employed standard nematode culture conditions [23]. All strains were maintained at 20 °C on Nematode Growth Media agar supplemented with Escherichia coli (OP50 or transformed HT115), unless otherwise indicated. Strains used in this work are listed in Supplementary Methods. All our neuromuscular and mitochondrial assays are carried out on L3 larvae unless otherwise specified.

RNAi feeding

The following dsRNA transformed bacteria for feeding were derived from the Ahringer *C. elegans* RNAi library [83]: *nuo-1* (C09H10.3), T20H4.5, F53F4.10, *cco-1* (F26E4.9), *nuo-5* (Y45G12B.1), *nuo-2* (T10E9.7), *spg-7* (Y47G6A.10), *lpd-5* (ZK973.10). For additional RNAi used in the phenotypic screening described in the text refer to Table S2 and S3. All dsRNA bacterial clones (sequence validated), were grown to a concentration of 0.9 OD and diluted 1/10 or 1/50 with empty vector expressing bacteria as previously described [18].

Lifespan assay

Lifespan and Statistical Survival analysis using synchronous populations of at least 60 animals per strain. Survival curves and statistical analyses were carried out as previously described [19]. See Table S2 and S3 for the summary of lifespan and Supplementary Methods for details.

Chemotaxis assay

Animal's sensory neurons functionality was assessed by quantifying attraction or repulsion to different concentration of chemicals as previously described as previously described [23]. See

also Supplementary Methods. Compounds used in chemotaxis assays were all acquired from Sigma-Aldrich: ammonium acetate (**A1542)**, was diluted in distillated water and 2-Methyl-3-(methylthio)pyrazine (**545791)**, 1-Butanol (**B7906)**, Benzaldehyde (**418099)**, all diluted in Ethanol 99.8%.

Body bend

Locomotion was assessed by counting the number of body bends (changes in the body bend at the mid-body point per minute), per minute for each worm on solid agar plates with no bacteria. One bend was counted every time the mid-body reached a maximum bend in the opposite direction from the bend last counted. Body bends were checked in at least 20 single worms in 2 or 3 independent biological trials [23].

Thrashing assay

To further define neuro-muscular differences on an individual level, we analyzed the swimming behavior (also known as thrashing) [84] of *nuo-5* animals. Age-synchronized worms were transferred to a fresh unseeded plate at room temperature to remove leftover bacteria; then individual worms were transferred to an unseeded small NGM plate filled with 1 mL of S-Basal buffer. Worms were allowed to acclimatize for 5 minutes, and the number of completed thrashes per minute was counted using a hand counter. This was performed on 15 individual worms per replicate in 2 or 3 independent biological trials.

Pharyngeal pumping

Pharyngeal pumping was measured using the ScreenChip^{TM} System (InVivo Biosystems). This platform allows to record the voltage changes caused by the contraction of the pharynx in real time, producing the so-called electropharyngeogram (EPG) [85]. The following parameters were measured: pump frequency, pump waveform shape, spike amplitude ratios, pump duration, interpump interval (IPI) and R to E ratio. (**Fig S12B** shows a representative EPG). Nematodes were washed off the plates with M9 and collected in a reaction tube as adults in the parental generation instead of L3. This technical adjustment was necessary since the size of the cartridges are to date not compatible with the size of our L3 larvae (the channels in the SC20 are too big while S30 are too small). Then, the worms were washed three times with M9 and incubated in a 10 mM serotonin solution (Sigma Aldrich, 14927) for 30 min. Worms were loaded on the ScreenChip SC40 with a syringe (0.01 ml – 1 ml). The EPG of single worms was recorded for a

duration of about 2 minutes. Only worms which showed pumping activity were recorded, while those with no pumping activity were discarded. The software programs NemAcquire 2.1, and NemAnalysis 0.2 (https://invivobiosystems.com/product-category/instruments/screenchip-system-software/) were used for recording and analysis respectively.

Aldicarb-induced paralysis

The assay was carried out as previously described [47]. We used plates containing either 0.5 mM or 1 mM final aldicarb (33386 Sigma-Aldrich) concentration in the NGM. Briefly, the animals were all L2/L3 larvae on one day of the assay; they were grown on RNAi plates before the beginning of the assay when 25/30 worms were transferred on a small spot (4 µl) of OP50 *E. coli* in the center of the agar plate. The small spot concentrates the animals into a small single field of view, thus making it easier for careful examination of all animals on a plate. After placing the animals on to an Aldicarb plate they were left at RT. Every 30 min, for a total of 5.5 hours, the worms were assayed for paralysis. We define a worm as paralyzed by the absence of movement when prodded three times with a platinum wire on the head and tail.

Levamisole-induced paralysis

The assay was carried out as previously described [48]. We used 50 µM final concentration. The levamisole stock solution (100 mM in $_{dd}H_20$) was added to the liquid NGM. The assay was performed similarly to the aldicarb with the only difference that the paralysis was scored every 15 minutes for 3 hours.

(PTZ)-induced paralysis

PTZ sensitivity assay was executed as previously described [49]. Briefly, 75 µl of a 100 mg/mL stock solution (in $_{dd}$H20) was added to plates containing 3 mL of solid NGM, making a final concentration of 2,5 mg/ml. The PTZ plates were allowed to dry for roughly 60-120 minutes at RT with the lids open. The assay was carried out as the aldicarb assay, with the difference that the animals were scored for head convulsions and full-body paralysis after 30 minutes and at one hour. The *C. elegans* strain *unc-49*(e407) was used as positive control. This GABAergic mutant shows significantly more anterior convulsion and full-body paralysis compared to wild-type animals (as far as our observations and as described in [86]).

Mitochondrial Respiration

Basal oxygen consumption rate (OCR), maximal respiratory capacity, spare respiratory capacity, ATP coupled respiration and proton leak, have been assessed as previously described [20]; all measurements were performed with synchronized L2-L3 *C. elegans*. See Supplementary Methods for details.

ATP levels

The intracellular ATP levels were assessed quantifying whole animal luminescence in the *C. elegans* strain PE255 as previously described [87].

Mitochondrial DNA copy number, mitochondrial DNA and nuclear DNA damage

nDNA and mtDNA damage have been evaluated using a quantitative PCR (QPCR)-based method as previously described [88].

Reactive oxygen species

Synchronous L3 stage worm populations of each strain were grown on NGM plates spread with RNAi bacteria and 10 µM MitoSOX Red (Molecular Probes, Eugene, OR). After 24-hour incubation, nematodes were transferred to fresh NGM RNAi plates for one hour to clear their guts of residual dye. Living nematodes were paralyzed *in situ* by directly adding 1 mg/ml levamisole to NGM agar plates. Photographs were taken immediately in the dark using a CY3 fluorescence filter. Subsequently, the terminal pharyngeal bulb (PB) was manually circled to quantify the region's mean intensity using ImageJ software (http://rsbweb.nih.gov/ij/).

Phenotype-based suppressor screening

The screen was run in 12-well plates. Each well contained 2 ml solid NGM+50 µL UV killed bacteria lawn+50 µl drug solution in final 0.25% DMSO. In each plate 3 wells were used for RNAi without any compound (0.25% DMSO as control) to check the efficacy of the RNAi on the vehicle; and 3 wells for pL4440 RNAi to have a negative control of animal development on the empty vector (**Fig S5B**). The screening was repeated for each compound between 1 (in case they gave 0 rescue in the first trial) and 5 times (in case we observed a rescue of the arrested development). Approximately 40 eggs were placed in each well and their development was observed every day until the animals became gravid adults (for a maximum of 6 days).

Quantification of Gene Expression through fluorescent transgene reporters

The effect of *nuo-5* and *lpd-5* RNAi and/or lutein treatment on the induction of different transgenic strains was investigated on synchronized population of L3 worms (unless otherwise indicated). The nematodes were placed in a 14µl S-Basal drop on a microscope glass slide, anesthetized with NaN_3 10mM, covered with a cover slide and immediately imaged. Pictures were acquired with an Imager2 Zeiss fluorescence microscope, magnification 10-fold. In each experiment a minimum of 15 to 20 animals per condition were used. Details for each fluorescent strain are described in Supplementary Methods.

RNA extraction and Microarray

Total RNA was extracted according to [34]. Details are described in Supplementary Methods. Quality control, hybridization and Affymetrix *C. elegans* Gene 1.0 ST Microarrays scanning were performed at the Center for Biological and Medical Research (BMFZ), Facility of the Heinrich Heine University of Düsseldorf. Results in **Fig 4** were obtained by raw data (Affymetrix.cel-files) preprocessing and analysis using R version 3.5.1 (2018-07-02). The data were RMA normalized by the oligo package and annotated using pd.elegene.1.0.st package [89]. The list of differentially expressed genes (DEG) was obtained using limma package [90] with FDR correction using a cut-off of adjusted p-value<0.05. The list of unfiltered differentially expressed genes was plot as enhanced volcano with cut-off 1 for log2FC and 10^{-6} for P value (**Fig 4B,C**). Results in **Fig 5** were obtained analysing the data with Partek Flow (build 7.0.18.1116). The data were RMA normalized and annotated using the STAR module. The list of differentially expressed genes (DEG) was obtained by ANOVA filtering with FDR correction using the GSA module with a cut-off of adjusted p-value<0.05. The list of DEG between *nuo-5* and *nuo-5* lutein treated worms was used to perform unsupervised Euclidian hierarchical clustering. The fold changes are represented as log2FC (base-2 logarithm of the fold change). Venn diagrams (**Fig 4A** and **5A**) and pathways representative for a selected list of genes were visualized as network plot of enriched terms in **Fig 5C** was created with ClueGO v2.5 [91], and statistical test used was enrichment/depletion (Two-sided hypergeometric test). The correction method used was Bonferroni step down. The network plots of enriched terms in **Fig 4F,G** and **Fig S9** were created in R, using Bioconductor [92]. Specifically, cnetplot function was used to extract the complex association [93]. R version 3.5.1 (2018-07-02), clusterProfiler_3.8.1, enrichplot_1.0.2, Bioconductor version 3.8.

RNA extraction and quantitative RT-PCR

Total RNA extraction was performed as described for the microarray. 3 biological replicas were collected to extract the total RNA and the cDNA was synthetized using GoScript™ Reverse Transcription Mix (Promega A2790). Primer pairs used for the qPCR are listed in **Table S10**.

Synchrotron Fourier Transform Infrared Microspectroscopy (SR-µFTIR)

Eggs were placed on agar plates (with or without lutein) and worms collected at L3 stage (stored at 20ºC). After washing three times with MilliQ water, worms were transferred to CaF_2 windows and dried in vacuum condition. µFTIR experiments were performed at the MIRAS beamline at ALBA synchrotron, using a Hyperion 3000 Microscope coupled to a Vertex 70 spectrometer (Brucker) equipped with 36x magnification objective. The measuring range was 650−4000 cm^{-1} and the spectra collection was done in transmission mode at 4 cm^{-1} spectral resolution. For single point measurements, a mercury cadmium telluride (MCT) detector was used with an aperture dimension of 10 µm × 10 µm and synchrotron light was used co-adding from 128-256 scans. Background spectra were collected from a clean area of each CaF2 window. A focal plane array (FPA) detector was used for imaging measurement using the internal source co-adding 256 scans. FTIR data was analysed using OPUS 7.5 (Brucker), Unscrambler 10.5 and Matlab R2010b (Mathworks). Spectra exhibiting low signal to noise ratio or saturation were deleted. Remaining spectra were corrected for Resonant Mie Scattering by an open-source algorithm provided by Gardner group [94]. Matrigel was used as reference spectrum, 10 iterations, a scattering particle diameter between 2-18 µm and a refractive index 1.1-1.5. A second-order Savitsky-Golay derivative with 9 smoothing points and a polynomial order of two was applied to the corrected data to eliminate baseline effects and improve peak resolution. Lipid oxidation, amide oxidation and lutein ratio were addressed by calculating the absorption ratios for each spectrum, v_s(C=O) 1745 cm^{-1} /v_{as} (CH_2) 2921 cm^{-1}, v_{as} (C=O) 1745 cm^{-1}/v_s(Amide) 1654 cm^{-1} and v(Lutein) 1515 cm^{-1}/v_{as} (CH_2) 2921 cm^{-1}.

Mouse methods

Ndufs4 knock out mouse brain sample preparation

All ethical regulations regarding animal handling and maintenance were followed. The mice were analyzed at 6 weeks of age [95]. The brains from 3 wt and 3 KO mice were collected for RNA analysis as previously described [96]. For q-RT-PCR experiments, mouse cortex tissues

were harvested, snap frozen in liquid nitrogen and stored at −80°C. Briefly, mice were anesthetized with isofluorane and euthanized by cervical dislocation. Mouse brains were rinsed in PBS, transferred into tubes and snap frozen in liquid nitrogen. These samples were frozen at −80°C until processed.

Quantitative RT-PCR

Tissue RNA was extracted with TriReagent (Sigma, T9424) according to supplier instructions. RNA concentration and quality were determined using Nanodrop (PeqLab) and cDNA was synthesized with the iScript cDNA synthesis kit (Bio-Rad) following manufacturer's protocol. Each 9 µl reaction for q-RT-PCR was made of 4 µl diluted cDNA, 0.25 µl of each primer (from 25 µM stock) and 4.5 µl of Luna Universal Master Mix (New England Biolabs). The q-RT-PCR reactions were run on the QuantStudio 6 Flex Real-Time PCR system (Applied Biosystems). qPCR results were analyzed using the DDCt method relative to the mean of housekeeping genes (Hprt, Gapdh and ActB). Each biological data point represents the average of three technical triplicates. Primer pairs used are listed in **Table S10**.

Human cells methods

Cells and culture conditions

Primary human skin fibroblasts (NHDF-neo, Lot Nr.: 7F3956; Lonza) were used as control cell line. Cell culture model systems of NDUFS4 and NDUFS1 deficiency included a primary human skin fibroblast cell line from a patient with a homozygous nonsense mutation c.20C>G; p.(Ser7*) in NDUFS4 (NM_002495.2) and a primary human skin fibroblast cell line from a patient with a compound-heterozygous mutation c.1855G>A; c.1669C>T in NDUFS1. All fibroblasts cell lines were cultured in DMEM with GlutaMAX™-I (Gibco by life technologies) supplemented with 10% FBS and 1% penicillin-streptomycin (5,000U/ml). Medium was replaced every 2-3 days and cells were split when the desired confluence (70-90%) had been reached.

Measurement of ROS levels

Specific measurements of mitochondrial ROS levels were performed with some modifications as described before [97]. Briefly, cells were cultured on glass bottom dishes (27 mm; Nunc by Thermo Fisher Scientific) in DMEM with GlutaMAX™-I (low glucose, Gibco by life technologies) supplemented with 10% FBS and 1% penicillin-streptomycin (5,000U/ml). Either

lutein (10 µM, 20 µM or 40µM; Sigma) or vehicle (0,1%, 0,2% or 0,4% dimethyl sulfoxide, DMSO, Sigma) was added to the culture medium and cells were cultured for 24 h, 48 h and 72 h in a humidified atmosphere (95% air, 5% CO2) at 37°C. Next, cells were incubated with MitoSOX ™ Red (5 µM, 10 min, 37°C; Invitrogen). The red fluorescence was documented using an Axio Observer Z1 microscope (Zeiss) with the dehydroethidium filter set (F39-500, F48-515, F47-895; AHF Analysetechnik). A minimum of 100 cells were analyzed per condition. Images were analyzed and fluorescence intensity was quantified using ImageJ software (http://rsbweb.nih.gov/ij/).

Statistical analysis

Data are represented as mean ± SEM from at least three independent biological replica carried out in a blinded manner where possible. Statistical analyses were performed using either two-sided Student's t-test, one-way ANOVA for multiple comparisons, or two-way ANOVA followed by Tukey's multiple-comparisons test for multiple comparisons and time-points. GraphPad Prism 6 software was used for all statistical analysis to calculate significance as follows: *p = 0.01 to 0.05, **p = 0.001 to 0.01, ***p = 0.0001 to 0.001, and ****p < 0.0001 versus respective control conditions.

Acknowledgment

We would like to thank Prof. Johnson at the University of Boulder and Prof. Rea (now at Washington University) for the possibility to carry out the initial customized HMAD RNAi screening. We also thank Dr Kell, Ms Cho and Dr Torgovnick for technical help with RNAi screen and lifespan. We thank Prof. Proksch at HHU for providing us with the compound library used in the suppressor screen, Núria Benseny-Cases at MIRAS beamline in ALBA Synchrotron Light Source, Cerdanyola del Vallès in Barcelona and Genis Rabost for technical assistance with FTIR measurements and analysis. We also thank Anthony Luz for assistance with the Seahorse XFe24 analysis in *C. elegans*, Ian Ryde for support with the DNA damage assays and Dirk Schwitters for qPCR on brains from WT and NDUFS4$^{-/-}$ mice. Finally, we thank the Caenorhabditis Genetics Center (funded by the National Institutes of Health Office of Research Infrastructure Programs: P40OD010440) as well as the National Bioresource Project (NBRP) for *C. elegans* strains and Professors Sieburth, Kaplan and Calahorro for providing additional mutants used in this work. The Wood-Whelan fellowship covered Silvia Maglioni costs to visit

Prof Meyer Laboratory. This work was possible thanks to financial support to NV from: the German Research Foundation (DFG grants VE663-3/1 and VE663/8-1), the Federal Ministry of Education and Research (JPI-HDHL, Grant no. 01EA1602), the Heinrich Heine University of Duesseldorf (Strategic Research Funding 2014). JNM acknowledges funding from the National Institutes of Health (P42ES010356). ZL acknowledges the fellowship from China Scholarship Council (CSC201607030005) and AL acknowledges the financial support from the Spanish Ministry of Science, Innovation and Universities (RTI2018-096273-B-I00) and the 'Severo Ochoa' Programme for Centers of Excellence in R&D (SEV-2015-0496). NR acknowledges the ERC Stg 337327 MitoPexLyso.

Author contributions

NV conceived and supervised the study. SM and NV designed the experiments. SM, MM, LZ and VB performed the experiments. SM, NV, MM, LZ, AS, NR analyzed the data. SM and NV wrote the paper. FD, AL, NR, JM edited the manuscript.

Conflict of interest

The authors declare no competing interests

Data availability

The data that support the findings of this study are available from the corresponding author upon reasonable request. The GEO accession numbers for microarray data reported in this paper are GSE144573 and GSE144574. Cell lines were obtained from patient-derived primary human skin fibroblasts. Ethical approval and patient consent for their use was obtained. Cell lines are available from the authors upon reasonable request.

References

1. Kwong, J.Q., M.F. Beal, and G. Manfredi, *The role of mitochondria in inherited neurodegenerative diseases.* J Neurochem, 2006. **97**(6): p. 1659-75.
2. Distelmaier, F., et al., *Mitochondrial complex I deficiency: from organelle dysfunction to clinical disease.* Brain, 2009. **132**(Pt 4): p. 833-42.
3. Chinnery, P.F., *Mitochondrial Disorders Overview*, in *GeneReviews(R)*, R.A. Pagon, et al., Editors. 2014: Seattle (WA).

4. Baertling, F., et al., *A guide to diagnosis and treatment of Leigh syndrome.* J Neurol Neurosurg Psychiatry, 2014. **85**(3): p. 257-65.
5. Silverman, G.A., et al., *Modeling molecular and cellular aspects of human disease using the nematode Caenorhabditis elegans.* Pediatr Res, 2009. **65**(1): p. 10-8.
6. Ventura, N., S.L. Rea, and R. Testi, *Long-lived C. elegans mitochondrial mutants as a model for human mitochondrial-associated diseases.* Exp Gerontol, 2006. **41**(10): p. 974-91.
7. O'Reilly, L.P., et al., *C. elegans in high-throughput drug discovery.* Adv Drug Deliv Rev, 2014. **69-70**: p. 247-53.
8. Artal-Sanz, M., L. de Jong, and N. Tavernarakis, *Caenorhabditis elegans: a versatile platform for drug discovery.* Biotechnol J, 2006. **1**(12): p. 1405-18.
9. Maglioni, S., N. Arsalan, and N. Ventura, *C. elegans screening strategies to identify pro-longevity interventions.* Mech Ageing Dev, 2016. **157**: p. 60-69.
10. Lublin, A.L. and C.D. Link, *Alzheimer's disease drug discovery: in vivo screening using Caenorhabditis elegans as a model for beta-amyloid peptide-induced toxicity.* Drug Discov Today Technol, 2013. **10**(1): p. e115-9.
11. Alexander, A.G., V. Marfil, and C. Li, *Use of Caenorhabditis elegans as a model to study Alzheimer's disease and other neurodegenerative diseases.* Front Genet, 2014. **5**: p. 279.
12. Teschendorf, D. and C.D. Link, *What have worm models told us about the mechanisms of neuronal dysfunction in human neurodegenerative diseases?* Mol Neurodegener, 2009. **4**: p. 38.
13. Helmcke, K.J., D.S. Avila, and M. Aschner, *Utility of Caenorhabditis elegans in high throughput neurotoxicological research.* Neurotoxicol Teratol, 2010. **32**(1): p. 62-7.
14. Maglioni, S. and N. Ventura, *C. elegans as a model organism for human mitochondrial associated disorders.* Mitochondrion, 2016.
15. Polyak, E., et al., *N-acetylcysteine and vitamin E rescue animal longevity and cellular oxidative stress in pre-clinical models of mitochondrial complex I disease.* Mol Genet Metab, 2018. **123**(4): p. 449-462.
16. Ventura, N. and S.L. Rea, *Caenorhabditis elegans mitochondrial mutants as an investigative tool to study human neurodegenerative diseases associated with mitochondrial dysfunction.* Biotechnol J, 2007. **2**(5): p. 584-95.
17. Hartman, P.S., et al., *Mitochondrial mutations differentially affect aging, mutability and anesthetic sensitivity in Caenorhabditis elegans.* Mech Ageing Dev, 2001. **122**(11): p. 1187-201.
18. Rea, S.L., N. Ventura, and T.E. Johnson, *Relationship between mitochondrial electron transport chain dysfunction, development, and life extension in Caenorhabditis elegans.* PLoS Biol, 2007. **5**(10): p. e259.
19. Ventura, N., et al., *p53/CEP-1 increases or decreases lifespan, depending on level of mitochondrial bioenergetic stress.* Aging Cell, 2009. **8**(4): p. 380-93.
20. Maglioni, S., et al., *Mitochondrial bioenergetic changes during development as an indicator of C. elegans health-span.* Aging (Albany NY), 2019. **11**(16): p. 6535-6554.
21. Tsang, W.Y. and B.D. Lemire, *Mitochondrial genome content is regulated during nematode development.* Biochem Biophys Res Commun, 2002. **291**(1): p. 8-16.
22. Ndegwa, S. and B.D. Lemire, *Caenorhabditis elegans development requires mitochondrial function in the nervous system.* Biochem Biophys Res Commun, 2004. **319**(4): p. 1307-13.
23. Maglioni, S., et al., *Mitochondrial stress extends lifespan in C. elegans through neuronal hormesis.* Exp Gerontol, 2014. **56**: p. 89-98.
24. Gorman, G.S., et al., *Perceived fatigue is highly prevalent and debilitating in patients with mitochondrial disease.* Neuromuscul Disord, 2015. **25**(7): p. 563-6.
25. Matthies, D.S., et al., *The Caenorhabditis elegans choline transporter CHO-1 sustains acetylcholine synthesis and motor function in an activity-dependent manner.* J Neurosci, 2006. **26**(23): p. 6200-12.

26. Gabaldon, T., D. Rainey, and M.A. Huynen, *Tracing the evolution of a large protein complex in the eukaryotes, NADH:ubiquinone oxidoreductase (Complex I).* J Mol Biol, 2005. **348**(4): p. 857-70.
27. Ni, Y., et al., *Mutations in NDUFS1 Cause Metabolic Reprogramming and Disruption of the Electron Transfer.* Cells, 2019. **8**(10).
28. Ugalde, C., et al., *Differences in assembly or stability of complex I and other mitochondrial OXPHOS complexes in inherited complex I deficiency.* Hum Mol Genet, 2004. **13**(6): p. 659-67.
29. Mango, S.E., *The C. elegans pharynx: a model for organogenesis.* WormBook, 2007: p. 1-26.
30. Brinkmann, V., et al., *Dietary and environmental factors have opposite AhR-dependent effects on C. elegans healthspan.* Aging (Albany NY), 2020. **13**(1): p. 104-133.
31. Meyer, J.N., et al., *Mitochondria as a target of environmental toxicants.* Toxicol Sci, 2013. **134**(1): p. 1-17.
32. Meyer, J.N., T.C. Leuthner, and A.L. Luz, *Mitochondrial fusion, fission, and mitochondrial toxicity.* Toxicology, 2017. **391**: p. 42-53.
33. Yoneda, T., et al., *Compartment-specific perturbation of protein handling activates genes encoding mitochondrial chaperones.* Journal of cell science, 2004. **117**(Pt 18): p. 4055-66.
34. Schiavi, A., et al., *Autophagy induction extends lifespan and reduces lipid content in response to frataxin silencing in C. elegans.* Exp Gerontol, 2013. **48**(2): p. 191-201.
35. Liu, Y., et al., *Caenorhabditis elegans pathways that surveil and defend mitochondria.* Nature, 2014. **508**(7496): p. 406-10.
36. Lapierre, L.R., et al., *The TFEB orthologue HLH-30 regulates autophagy and modulates longevity in Caenorhabditis elegans.* Nat Commun, 2013. **4**: p. 2267.
37. Maglioni, S., et al., *An automated phenotype-based microscopy screen to identify pro-longevity interventions acting through mitochondria in C. elegans.* Biochim Biophys Acta, 2015. **1847**(11): p. 1469-78.
38. *Carotenoids. Volume 1B: Spectroscopy*. 1995, Basel: Birkhäuser Verlag AG. xvi + 360 pp.
39. Santocono, M., et al., *Influence of astaxanthin, zeaxanthin and lutein on DNA damage and repair in UVA-irradiated cells.* J Photochem Photobiol B, 2006. **85**(3): p. 205-15.
40. Swanson HM, S.J., Gong X, Rubin LP, *Lutein, but not other carotenoids, selectively inhibits breast cancer cell growth through several molecular mechanisms.* FASEB J, 2016: p. 30(1 Suppl):34.2.
41. Liu, R., et al., *Lutein and zeaxanthin supplementation and association with visual function in age-related macular degeneration.* Invest Ophthalmol Vis Sci, 2014. **56**(1): p. 252-8.
42. Kiko, T., et al., *Significance of lutein in red blood cells of Alzheimer's disease patients.* J Alzheimers Dis, 2012. **28**(3): p. 593-600.
43. Sujak, A., et al., *Lutein and zeaxanthin as protectors of lipid membranes against oxidative damage: the structural aspects.* Arch Biochem Biophys, 1999. **371**(2): p. 301-7.
44. Cristina, D., et al., *A regulated response to impaired respiration slows behavioral rates and increases lifespan in Caenorhabditis elegans.* PLoS Genet, 2009. **5**(4): p. e1000450.
45. Baruah, A., et al., *CEP-1, the Caenorhabditis elegans p53 homolog, mediates opposing longevity outcomes in mitochondrial electron transport chain mutants.* PLoS Genet, 2014. **10**(2): p. e1004097.
46. Oh, K.H. and H. Kim, *Aldicarb-induced Paralysis Assay to Determine Defects in Synaptic Transmission in Caenorhabditis elegans.* Bio Protoc, 2017. **7**(14).
47. Mahoney, T.R., S. Luo, and M.L. Nonet, *Analysis of synaptic transmission in Caenorhabditis elegans using an aldicarb-sensitivity assay.* Nat Protoc, 2006. **1**(4): p. 1772-7.
48. Mulcahy, B., L. Holden-Dye, and V. O'Connor, *Pharmacological assays reveal age-related changes in synaptic transmission at the Caenorhabditis elegans neuromuscular junction that are modified by reduced insulin signalling.* J Exp Biol, 2013. **216**(Pt 3): p. 492-501.

49. Locke, C., et al., *Paradigms for pharmacological characterization of C. elegans synaptic transmission mutants.* J Vis Exp, 2008(18).
50. Thapliyal, S. and K. Babu, *Pentylenetetrazole (PTZ)-induced Convulsion Assay to Determine GABAergic Defects in Caenorhabditis elegans.* Bio Protoc, 2018. **8**(17).
51. Fleming, J.T., et al., *Caenorhabditis elegans levamisole resistance genes lev-1, unc-29, and unc-38 encode functional nicotinic acetylcholine receptor subunits.* J Neurosci, 1997. **17**(15): p. 5843-57.
52. Lemons, M.L., *An Inquiry-Based Approach to Study the Synapse: Student-Driven Experiments Using C. elegans.* J Undergrad Neurosci Educ, 2016. **15**(1): p. A44-A55.
53. Weimer, R.M., et al., *UNC-13 and UNC-10/rim localize synaptic vesicles to specific membrane domains.* J Neurosci, 2006. **26**(31): p. 8040-7.
54. Meissner, B., et al., *Determining the sub-cellular localization of proteins within Caenorhabditis elegans body wall muscle.* PLoS One, 2011. **6**(5): p. e19937.
55. Sandoval, G.M., et al., *A genetic interaction between the vesicular acetylcholine transporter VAChT/UNC-17 and synaptobrevin/SNB-1 in C. elegans.* Nat Neurosci, 2006. **9**(5): p. 599-601.
56. Hu, Z., et al., *Neurexin and neuroligin mediate retrograde synaptic inhibition in C. elegans.* Science, 2012. **337**(6097): p. 980-4.
57. Staab, T.A., et al., *Regulation of synaptic nlg-1/neuroligin abundance by the skn-1/Nrf stress response pathway protects against oxidative stress.* PLoS Genet, 2014. **10**(1): p. e1004100.
58. Calahorro, F. and M. Ruiz-Rubio, *Functional phenotypic rescue of Caenorhabditis elegans neuroligin-deficient mutants by the human and rat NLGN1 genes.* PLoS One, 2012. **7**(6): p. e39277.
59. Silva-Pinheiro, P., et al., *A Single Intravenous Injection of AAV-PHP.B-hNDUFS4 Ameliorates the Phenotype of Ndufs4 (-/-) Mice.* Mol Ther Methods Clin Dev, 2020. **17**: p. 1071-1078.
60. Dell'agnello, C., et al., *Increased longevity and refractoriness to Ca(2+)-dependent neurodegeneration in Surf1 knockout mice.* Hum Mol Genet, 2007. **16**(4): p. 431-44.
61. Inak, G., et al., *Defective metabolic programming impairs early neuronal morphogenesis in neural cultures and an organoid model of Leigh syndrome.* Nat Commun, 2021. **12**(1): p. 1929.
62. Dillin, A., et al., *Rates of behavior and aging specified by mitochondrial function during development.* Science, 2002. **298**(5602): p. 2398-401.
63. Bennett, C.F., et al., *Activation of the mitochondrial unfolded protein response does not predict longevity in Caenorhabditis elegans.* Nat Commun, 2014. **5**: p. 3483.
64. Bjorkman, K., et al., *Broad phenotypic variability in patients with complex I deficiency due to mutations in NDUFS1 and NDUFV1.* Mitochondrion, 2015. **21**: p. 33-40.
65. Luz, A.L., et al., *Deficiencies in mitochondrial dynamics sensitize Caenorhabditis elegans to arsenite and other mitochondrial toxicants by reducing mitochondrial adaptability.* Toxicology, 2017. **387**: p. 81-94.
66. Muraresku, C.C., E.M. McCormick, and M.J. Falk, *Mitochondrial Disease: Advances in clinical diagnosis, management, therapeutic development, and preventative strategies.* Curr Genet Med Rep, 2018. **6**(2): p. 62-72.
67. Devine, M.J. and J.T. Kittler, *Mitochondria at the neuronal presynapse in health and disease.* Nat Rev Neurosci, 2018. **19**(2): p. 63-80.
68. Nikoletopoulou, V. and N. Tavernarakis, *Regulation and Roles of Autophagy at Synapses.* Trends Cell Biol, 2018. **28**(8): p. 646-661.
69. Schiavi, A., et al., *Iron-Starvation-Induced Mitophagy Mediates Lifespan Extension upon Mitochondrial Stress in C. elegans.* Curr Biol, 2015. **25**(14): p. 1810-22.
70. Matzinger, M., K. Fischhuber, and E.H. Heiss, *Activation of Nrf2 signaling by natural products-can it alleviate diabetes?* Biotechnol Adv, 2018. **36**(6): p. 1738-1767.

71. Hunter, J.W., et al., *Neuroligin-deficient mutants of C. elegans have sensory processing deficits and are hypersensitive to oxidative stress and mercury toxicity.* Dis Model Mech, 2010. **3**(5-6): p. 366-76.
72. Grella Miranda, C., et al., *Influence of nanoencapsulated lutein on acetylcholinesterase activity: In vitro determination, kinetic parameters, and in silico docking simulations.* Food Chem, 2020. **307**: p. 125523.
73. Nolan, J.M., et al., *The impact of supplemental macular carotenoids in Alzheimer's disease: a randomized clinical trial.* J Alzheimers Dis, 2015. **44**(4): p. 1157-69.
74. Desmidt, T., C. Hommet, and V. Camus, *Pharmacological treatments of behavioral and psychological symptoms of dementia in Alzheimer's disease: role of acetylcholinesterase inhibitors and memantine.* Geriatr Psychol Neuropsychiatr Vieil, 2016. **14**(3): p. 300-6.
75. Dufort-Gervais, J., et al., *Neuroligin-1 is altered in the hippocampus of Alzheimer's disease patients and mouse models, and modulates the toxicity of amyloid-beta oligomers.* Sci Rep, 2020. **10**(1): p. 6956.
76. Xue, C., et al., *Management of Ocular Diseases Using Lutein and Zeaxanthin: What Have We Learned from Experimental Animal Studies?* J Ophthalmol, 2015. **2015**: p. 523027.
77. Nataraj, J., et al., *Lutein protects dopaminergic neurons against MPTP-induced apoptotic death and motor dysfunction by ameliorating mitochondrial disruption and oxidative stress.* Nutr Neurosci, 2016. **19**(6): p. 237-46.
78. Arunkumar, R., et al., *Biodegradable Poly (Lactic-co-Glycolic Acid)-Polyethylene Glycol Nanocapsules: An Efficient Carrier for Improved Solubility, Bioavailability, and Anticancer Property of Lutein.* J Pharm Sci, 2015. **104**(6): p. 2085-2093.
79. Kamil, A., et al., *Bioavailability and biodistribution of nanodelivered lutein.* Food Chem, 2016. **192**: p. 915-23.
80. Andreux, P.A., et al., *A method to identify and validate mitochondrial modulators using mammalian cells and the worm C. elegans.* Sci Rep, 2014. **4**: p. 5285.
81. Andreux, P.A., R.H. Houtkooper, and J. Auwerx, *Pharmacological approaches to restore mitochondrial function.* Nat Rev Drug Discov, 2013. **12**(6): p. 465-83.
82. Jansen-Olesen, I., P. Tfelt-Hansen, and J. Olesen, *Animal migraine models for drug development: status and future perspectives.* CNS Drugs, 2013. **27**(12): p. 1049-68.
83. Kamath, R.S. and J. Ahringer, *Genome-wide RNAi screening in Caenorhabditis elegans.* Methods, 2003. **30**(4): p. 313-21.
84. Pierce-Shimomura, J.T., et al., *Genetic analysis of crawling and swimming locomotory patterns in C. elegans.* Proc Natl Acad Sci U S A, 2008. **105**(52): p. 20982-7.
85. Lockery, S.R., et al., *A microfluidic device for whole-animal drug screening using electrophysiological measures in the nematode C. elegans.* Lab Chip, 2012. **12**(12): p. 2211-20.
86. Dabbish, N.S. and D.M. Raizen, *GABAergic synaptic plasticity during a developmentally regulated sleep-like state in C. elegans.* J Neurosci, 2011. **31**(44): p. 15932-43.
87. Luz, A.L., et al., *In Vivo Determination of Mitochondrial Function Using Luciferase-Expressing Caenorhabditis elegans: Contribution of Oxidative Phosphorylation, Glycolysis, and Fatty Acid Oxidation to Toxicant-Induced Dysfunction.* Curr Protoc Toxicol, 2016. **69**: p. 25 8 1-25 8 22.
88. Meyer, J.N., *QPCR: a tool for analysis of mitochondrial and nuclear DNA damage in ecotoxicology.* Ecotoxicology, 2010. **19**(4): p. 804-11.
89. Carvalho, B.S. and R.A. Irizarry, *A framework for oligonucleotide microarray preprocessing.* Bioinformatics, 2010. **26**(19): p. 2363-7.
90. Ritchie, M.E., et al., *limma powers differential expression analyses for RNA-sequencing and microarray studies.* Nucleic Acids Res, 2015. **43**(7): p. e47.
91. Bindea, G., J. Galon, and B. Mlecnik, *CluePedia Cytoscape plugin: pathway insights using integrated experimental and in silico data.* Bioinformatics, 2013. **29**(5): p. 661-3.

92. Yu, G., *enrichplot: Visualization of Functional Enrichment Result. R package version 1.0.2.* 2018.
93. Team, R.C., *R: A Language and Environment for Statistical Computing*.
94. Bassan, P., et al., *Resonant Mie scattering (RMieS) correction of infrared spectra from highly scattering biological samples.* Analyst, 2010. **135**(2): p. 268-77.
95. Kruse, S.E., et al., *Mice with mitochondrial complex I deficiency develop a fatal encephalomyopathy.* Cell Metab, 2008. **7**(4): p. 312-20.
96. Fernandez-Mosquera, L., et al., *Mitochondrial respiratory chain deficiency inhibits lysosomal hydrolysis.* Autophagy, 2019. **15**(9): p. 1572-1591.
97. Distelmaier, F., et al., *Mitochondrial dysfunction in primary human fibroblasts triggers an adaptive cell survival program that requires AMPK-alpha.* Biochim Biophys Acta, 2015. **1852**(3): p. 529-40.

Tables

Table 1
List of genes whose different degree of silencing consistently led to the typical *Mit* phenotypes

Cosmid ID	Gene	Human ortholog, Short gene description	Disease	RNAi Power	Phenotype
ZK973.10	***lpd-5***	NDUFS4, NADH-Dehydrogenase, Fe-S protein complex I subunit	Complex I deficiency (Leigh Syndrome)	mild	few progeny
				strong	slow development; few eggs
Y45G12B.1	***nuo-5***	NDUFS1, NADH-Ubiquinone Oxidoreductase Fe-S Protein 1; complex I	Complex I deficiency (Leigh Syndrome)	mild	pale, small, few eggs
				strong	slow development, arrested L2/L3
C09H10.3	***nuo-1****	NDUFV1, mitochondrial NADH Dehydrogenase Ubiquinone Flavoprotein 1	Complex I deficiency (Leigh Syndrome)	mild	pale, thin, sterile
				strong	arrested as L2/L3
T20H4.5	**T20H4.5***	NDUFS8, ubiquinone oxidoreductase core subunit S8	Complex I deficiency (Leigh Syndrome)	mild	pale, thin, small, few eggs
				strong	arrested L2/L3
F53F4.10	**F53F4.10**	NDUFV2, Fe-S complex I	Complex I deficiency Parkinson's Disease Susceptibility	mild	slow development
				strong	slow development, arrested L2/L3
C01F1.2	***sco-1***	SCO-1, SCO cytochrome c oxidase assembly protein 1	Cytochrome-c oxidase deficiency disease	mild	pale, few progeny
				strong	slow development, sick, thin, sterile
H14A12.2	***fum-1***	FH, fumarate hydratase, predicted to have fumarate hydratase activity	Fumarase deficiency, Leigh Syndrome	mild	few eggs
				strong	few progeny, slow development
T12E12.4	***drp-1***	DNM1L (dynamin 1 like)	Optic Dystrophy	mild	similar to control
				strong	small, pale

D2013.5	***eat-3****	OPA-1 or *mgm*-1, dynamin family GTPase	Dominant Optic Atrophy	mild	thin
				strong	thin, slow development
F54H12.1	***aco-2***	ACO2, Mitochondrial aconitase	Infantile Cerebellar-Retinal Degeneration and Optic Atrophy 9	mild	few progeny
				strong	sterile
Y47G6A.10	***spg-7****	AFG3L2, AFG3 like matrix AAA peptidase subunit 2	Spinocerebellar ataxia (SCA28)	mild	pale, small, thin few eggs, few progeny
				strong	slow development, arrested L2
F23B12.5	***dlat-1****	DLAT, dihydrolipoamide S-acetyltransferase	pyruvate decarboxylase deficiency	mild	sterile, slow moving
				strong	sterile
K08E3.7	***pdr-1****	PARK-2 or parkin, E3 ubiquitin ligase	Parkinson's Disease	mild	slow moving, pale, few progeny
				strong	slow moving, pale, few eggs, protruding vulva
F25B4.6	***hmgs-1****	HMGCS1 & HMGCS2, 3-hydroxy-3-methylglutaryl-CoA synthase 1 & 2	Mitochondrial HMG-CoA Synthase Deficiency	mild	pale, thin, slow moving
				strong	sick, pale, slow moving
C15F1.7	***sod-1***	SOD-1, Cu-Zn SOD1	Amyotrophic lateral sclerosis	mild	small
				strong	similar to control
T22B11.5	***ogdh-1***	OGDH, predicted to have oxoglutarate dehydrogenase (succinyl-transferring) activity	Alpha ketoglutarate deficiency	mild	thin, pale, sterile adults
				strong	thin, pale, slow development, sick
W02F12.5	***dlst-1****	DLST, dihydrolipoamide S-succinyl transferase	Possible cause of familial Alzheimer's disease	mild	Skinny, pale
				strong	long, pale
Y46G5A.2	***cox-10***	COX10, complex IV farnesyl transferase	Mitochondrial complex IV deficiency	mild	few eggs, pale
				strong	Pale, few eggs
T27E9.1	***tag-61****	SLC25A5, solute carrier family 25 member 5, mitochondrial adenine nucleotide transporters	Mitochondrial Phosphate Carrier Deficiency	mild	thin, pale
				strong	small, pale, sterile,

					protruding vulva
F01F1.12	**aldo-2**	ALDOB, encodes a fructose-bisphosphate aldolase	Hereditary fructose intolerance	mild	pale
				strong	sick, pale

Genes in red are complex I genes giving a typical *Mit* mutants phenotype in our first screen, which we mainly followed up on in this study.

* These clones showed a strong phenotype already in the parental generation (P0, see **Fig 1**) when used undiluted, and the mild effect was thus achieved by diluting the dsRNA expressing bacteria (P0, 1/10 or 1/15). Lifespan for these clones were carried out accordingly in the parental generation (P0) left undiluted or diluted (**Table S2**).

For all the other clones a mild phenotype was observed in the undiluted parental generation (P0), while a strong one in the first filial generation (F1). Accordingly, lifespan with these clones were completed with P0 & F1on undiluted dsRNA expressing bacteria (**Table S3**). Nonetheless, since clones T20H4.5, *eat-3* and *spg-7* displayed a significant phenotype (but not as strong as others) already in the parental generation, their lifespan was assessed in P0/F1 as well as in diluted/undiluted conditions (see **Table S2** and **S3**).

Figures' legends

Figure 1. Phenotypic screening to identify *C. elegans* models for human mitochondrial-associated disorders.

A) At Day 0 animals were allowed to lay eggs on undiluted bacteria expressing dsRNA for each clone under study. Progeny development was observed for the following 3/4 days (P0 or parental generation). Three possible scenarios were then identified for the different RNAi clones. 1) No effect (black): worms reached adulthood in 3 days and looked similar to wild-type, control (empty-vector) treated worms. These clones were not subsequently followed. ii) A "mild" phenotype (light blue): decreased size and fertility and slow development were observed (representative images are shown in panels **B-C**). iii) A "strong" phenotype (dark blue): sterility, growth arrest or lethality were observed (representative images are shown in panels B-C). The clones giving a "mild" phenotype were followed in the next generation, in search of a strong effect (Day 6/7, F1 or first filial generation). If a strong phenotype was instead observed in the P0 then the RNAi bacteria were diluted with bacteria expressing empty vector (1:10 or 1:50), an egg lay was performed and the progeny was followed again in the P0 to identify a mild effect.

B-C) Screening representative pictures of different phenotypes induced by mild suppression of the listed genes (P0 in panel **B** or 1:10 dilution in panel **C**) or strong (F1 in panel **B** or undiluted in panel **C**), after 4 days from egg-lay. Mild genes suppression reduces adult animals' size and fertility rate. Strong gene suppression leads to animals early developmental arrest (F1, **B**) or sterility (undiluted, **C**). Two of the clones shown in **B** (i.e. *spg-7* and T20H4.5), already led to a significant effect in the parental generation (P0), and were therefore also diluted to achieve an even milder phenotype more similar to those shown in panel **C**. See also **Table 1** and **Supplementary Table 2** and **3**). See text for details. Pictures were acquired with a Leica MZ10 F modular stereo microscope connected to a color digital camera. Scale Bars 500 µm.

Figure 2. Severe suppression of Complex I genes significantly impairs sensory neurons and mitochondrial functionality.

Animals were fed bacteria transformed either with empty-vector (con) or with vector expressing dsRNA against *nuo-5* or *lpd-5*. **A-B**) Chemotaxis index reached after 240 minutes in response to 1% Butanol or 1% Pyrazine respectively. N=3, n=100-250 per group. **C**) Pharyngeal Pump frequency was measured using the ScreenChipTM System (InVivo Biosystems). N=2-5 n=15-20 **D-G**) Basal OCR, maximal OCR and ATP-linked OCR were measured using the Seahorse XF24 Analyzer while ATP production was measured using the luciferase-expressing strain PE255. N=3, n=1000-1500. **H**) ROS production was measured with MitoSOX Red. N=2, n=20-25. **I**) $P_{gst\text{-}4}$::GFP expression, N=4, n=10-20. **J**) $P_{hsp\text{-}6}$::GFP expression. N=4, n=15-20. **K**) $P_{dct\text{-}1}$::DCT-1::GFP expression. N=2, n=15-25. **L**) $P_{hlh\text{-}30}$::HLH-30::GFP expression. N=4, n=10-20. In all panels asterisks (*) denote statistical significance. *p-value <0.05 **p-value < 0.01, ***p-value < 0.001 ****p-value < 0.0001. Bar graphs represent means ± SEM**.** One-way ANOVA. N, number of trials. n, number of animals per trial.

Figure 3. Phenotype-based screening identifies lutein ability to rescues behavioral and cellular defects in models of Human Complex I deficiency.

A-B) Compounds rescuing more than 20% of the population. **a**) *p-value 0.0379 and ****p-value < 0.0001 compared to *nuo-5* RNAi in DMSO **b**) *p-value 0.022, **p-value 0.001, ****p-value < 0.0001 compared to *lpd-5* RNAi DMSO (N=2-4, n= 40), two-tailed Student's t-test **c**) Representative pictures of 4 wells of a 12-well plate 3 days after eggs hatching. Scale bars, 1 mm. **D**) Relative mRNA expression of *nuo-5* assessed by qPCR. **E**) Quantification of lutein

ratio addressed with the use of peak 1515.775^{cm-1} as Lutein's characteristic peak and ratio equation (Lutein/CH_2). Normalized on control values. Statistical analysis was carried out using one-way ANOVA. **F**,**H**) Chemotaxis curves and **G,I**) maximum chemotaxis index, reached after 240 minutes using as attractants **F,G**) 1 µl of 1% pyrazine or **H,I**)1 µl of 1% butanol. N=3, n=100-250, two-way ANOVA followed by Tukey's multiple-comparisons test. **J**) Pharyngeal pump frequency in adult worms fed for one generation with RNAi (N=2-3, n= 10-15), two-tailed Student's t-test.

K) ROS production, measured with MitoSOX Red, quantified in the pharyngeal bulb. N=2, n=20-25. **L**) Quantification of GFP nuclear translocation in a strain expressing the P_{hlh-30}::HLH-30::GFP transgene. N=4, n=10-20. **M**) ROS production in patients' derived skin fibroblasts after 24 hours incubation with lutein. Numerals reflect the number of individual cells analysed. N=3.

In **F**, **G**, **H**, **I, J, K** and **L** animals were fed bacteria transformed either with empty-vector (con) or with vector expressing dsRNA against *nuo-5* or *lpd-5* treated with lutein 1 µM (unless otherwise specified) or left untreated.

Bar graphs represent means ± SEM. Asterisks (*) denote significant differences vs control, # denote differences among conditions. One-way ANOVA unless otherwise indicated. *p-value <0.05 ** p value < 0.01, ***p-value < 0.001, ****p-value < 0.0001.

Figure 4. Mild and strong suppression of *nuo-5* lead to different gene expression profiles.

A) Venn diagram of the differentially altered genes identified in the microarray analysis. The transcriptomic profile in control L3 larvae was compared with that of mild or strong (arrested) *nuo-5* RNAi. **B-C**) Volcano plot displaying differential expressed genes between mild vs strong nuo-5 RNAi **B**) and strong nuo-5 RNAi vs control **C**). The vertical axis (y-axis) corresponds to the mean expression value of log 10 (q-value), and the horizontal axis (x-axis) displays the log 2-fold change value. Genes left to the vertical dashed line are down-regulated while genes right to the vertical dashed line are up-regulated. The horizontal dashed line separates significant differentially regulated genes (P cut-off 10-6). Total number of probes=29317. Grey dots between the two vertical dashed lines denote genes with no significant difference. Plots were designed in R, using Bioconductor. **D**) GO analysis of the 303 uniquely altered genes between mild vs strong *nuo-5* RNAi and **E**) of the 1152 genes uniquely altered between strong *nuo-5* RNAi vs control. **F**) Network plot of enriched terms between strong *nuo-5* RNAi vs control and **G**) for mild vs strong *nuo-5* RNAi were created in R, using Bioconductor. For statistical analysis

Enrichment/Depletion, two-sided hypergeometric test was used followed by correction with Bonferroni step down.

Figure 5. Microarray analysis of worms treated with bacteria expressing empty-vector control, or strong RNAi against *nuo-5* or *nuo-5* treated with lutein.

A) Venn diagram obtained using the online tool: http://bioinformatics.psb.ugent.be/webtools/Venn/.

B) Unsupervised hierarchical clustering of the transcripts corrected by treatment of the mutant *nuo-5* with 1 µM lutein. Each of the twelve lines represents a sample, and each of the columns represents a transcript (list of genes is **Table S8**). Expression levels (log2FC) are represented by a heatmap (the scale is included in the top-right quadrant, green represents down-regulation, min log2FC= -2.39; red represents up-regulation, max log2FC= 3.13).

The microarray data were obtained with a total of 16 *C. elegans* samples. The analysis included the 143 genes significantly differentially expressed between *nuo-5* vs *nuo-5* + lutein (light blue circle in the Venn diagram in panel (**A**). **C**) Log2FC (base-2 logarithm of the fold change) of *nuo-5* expression extracted from microarray data. **D-F**) gene expression from microarray data showing representative genes among those from the heatmap (**Fig 5B**) divided in three groups based on their expression levels: **D**) low (<10), **E**) middle (between 10 and 100) and **F**) high (>100) level.

G) Pathways enriched in the microarray *nuo-5* vs *nuo-5* + lutein designed using ClueGO v2.5.

Figure 6. Lutein suppresses an *nlg-1*-dependent synaptic defect in *nuo-5*-depleted animals.

Worms in all panels were fed bacteria transformed either with empty-vector (con, black bars) or with vector expressing dsRNA against *nuo-5* (light blue bars) and left untreated or treated with 1µM Lutein. **A**) Bars indicate percentage of animals paralyzed after 180 minutes on plates containing 0.5 mM aldicarb. N=3, n=25-30. **B**) Bars indicate percentage of animals paralyzed on plates containing 50 µM Levamisole. N=4, n=25-30. **C**) Bars indicate percentage of animals with the indicated phenotypes after 1 hour of exposure to 2.5 mg/ml PTZ. N=4, n=15-17. Asterisks denote the differences only of the full body-paralysis phenotype. **D-F**) Quantification of GFP expression in the indicated transgenic strains. N=3, n=20-35.

Bar graphs represent means ± SEM. Asterisks (*) denote significant differences vs control, # denote differences among conditions. *p-value <0.05 ** p value < 0.01, ***p-value < 0.001, ****p-value < 0.0001. One-way ANOVA unless otherwise indicated.

G-H) Fold change of genes involved in synaptic vesicle cycle expression (from microarray data).

Figure 7. Upregulation of neuroligin and neurexin genes upon *nuo-5* is conserved across species and the defect is rescued by lutein but no other antioxidants.

A) Expression levels of neuroligin (NLGN1-2 and 4) and neurexin (NRX1 and 3) transcripts in brains of NDUFS4-/- mice compared to healthy animals normalized to ACTB, assessed by qPCR. **B-C)** Fold change of genes described as *nlg-1* interactors (from microarray data). **D**) Quantification of GFP expression of p_{nlg-1} transgenic strain. N=3, n=15-20. **E)** Representative pictures of p_{nlg-1}::GFP in ventral nerve cord. Scale bar 10 µm. **F**) Sensitivity to Aldicarb. Bars indicate percentage of paralyzed animals after 180 minutes on plates containing 0,5 mM Aldicarb. Numerals reflect the number of individual nematodes analysed. N=2 to 3. **G**) Quantification of GFP expression in P*nlg*-1::gfp transgenic strain. N=3, n=20-35.

One-way ANOVA, bar graphs represent means ± SEM, asterisks (*) denote significant differences vs control, # denote differences among conditions. *p-value <0.05 ** p value < 0.01, ***p-value < 0.001, ****p-value < 0.0001.

Figure 8. Neuroligin mediates the protective effect of lutein on cholinergic synapses.

A) Frequency of body bends in liquid media ("thrashing") were quantified manually for one minute. N=3, n=15. **B**) Bars indicate percentage of animals paralyzed after 90 minutes on plates containing 0.5 mM aldicarb. N=3, n=25-30. **C**) Bars indicate percentage of animals paralyzed after 180 minutes on plates containing 50 µM Levamisole. N=4, n=25-30. **D**) Bars indicate the percentage of animals showing full-body paralysis after one hour of exposure to 2.5 mg/ml PTZ. N=4, n=15-17. **E**) Bars indicate the percentage of different developmental stages in wild-type and *nlg-1* mutants after 6 days from egg lay. Asterisks denote differences between the percentages of animals which reached the gravid adult (GA) stage. N=4, n=40, two-way ANOVA, followed by Tukey's multiple-comparisons test. **F**) Representative pictures of p_{nlg-1}::NLG-1::GFP in ventral nerve cord of adult and L3 larvae in the parental generation. Scale bar 10 µm **G**) Aldicarb sensitivity assay in the *nlg-1(ok259)* rescued by a p_{nlg-1}::NLG-1 transgene, bars indicate percentage of paralyzed animals after 120 minutes on plates containing 1 mM

aldicarb before paralysis. N=3, n=25-30. The assay was carried out using adult worms of the parental generation.

Figure 1

A

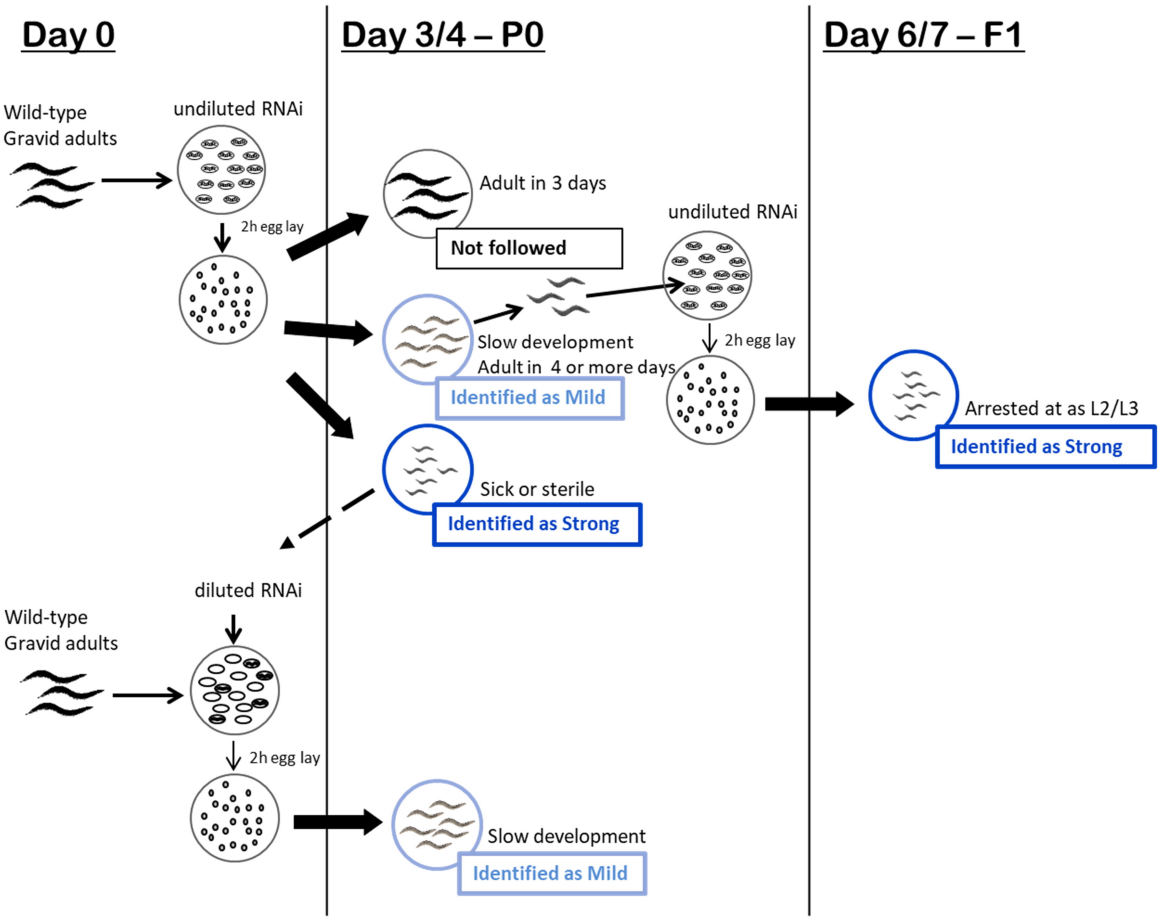
Day 0
Day 3/4 – P0
Day 6/7 – F1
Wild-type
Gravid adults
undiluted RNAi
2h egg lay
Adult in 3 days
Not followed
undiluted RNAi
Slow development
Adult in 4 or more days
Identified as Mild
2h egg lay
Arrested at as L2/L3
Identified as Strong
Sick or sterile
Identified as Strong
diluted RNAi
Wild-type
Gravid adults
2h egg lay
Slow development
Identified as Mild

B

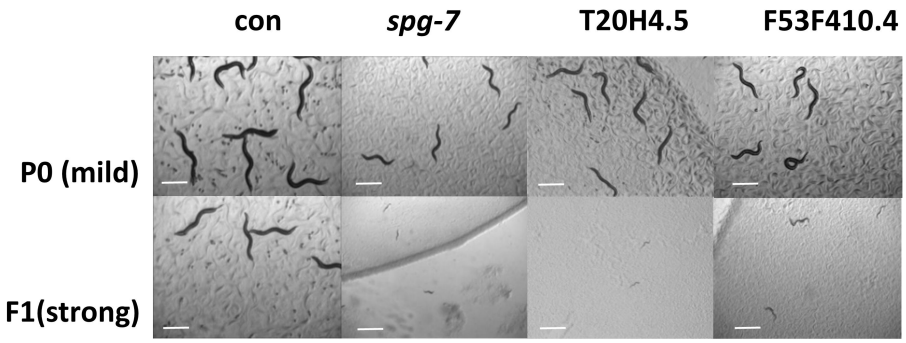
con
spg-7
T20H4.5
F53F410.4
P0 (mild)
F1(strong)

C

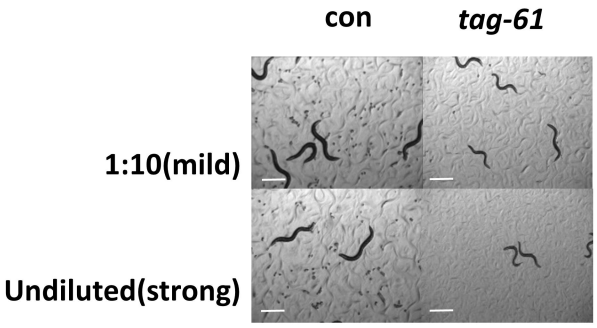
con
tag-61
1:10(mild)
Undiluted(strong)

Figure 2

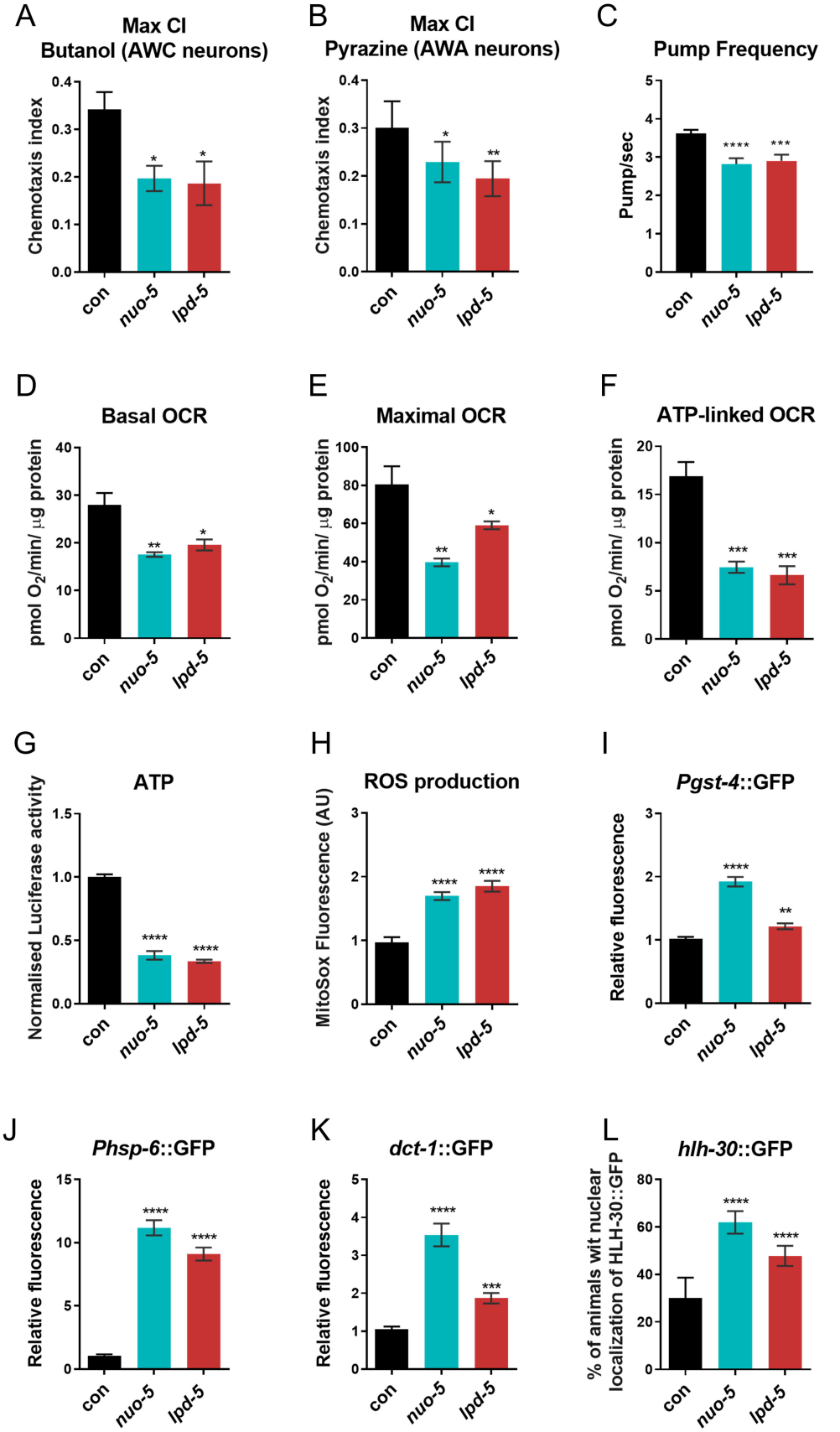
A
Max CI
Butanol (AWC neurons)
Chemotaxis index
0.0
0.1
0.2
0.3
0.4
*
*
con
nuo-5
lpd-5
B
Max CI
Pyrazine (AWA neurons)
Chemotaxis index
0.0
0.1
0.2
0.3
0.4
*
**
con
nuo-5
lpd-5
C
Pump Frequency
Pump/sec
0
1
2
3
4
5
****
***
con
nuo-5
lpd-5
D
Basal OCR
pmol O2/min/ µg protein
0
10
20
30
40
**
*
con
nuo-5
lpd-5
E
Maximal OCR
pmol O2/min/ µg protein
0
20
40
60
80
100
**
*
con
nuo-5
lpd-5
F
ATP-linked OCR
pmol O2/min/ µg protein
0
5
10
15
20
***
***
con
nuo-5
lpd-5
G
ATP
Normalised Luciferase activity
0.0
0.5
1.0
1.5
****
****
con
nuo-5
lpd-5
H
ROS production
MitoSox Fluorescence (AU)
0
1
2
3
****
****
con
nuo-5
lpd-5
I
Pgst-4::GFP
Relative fluorescence
0
1
2
3
****
**
con
nuo-5
lpd-5
J
Phsp-6::GFP
Relative fluorescence
0
5
10
15
****
****
con
nuo-5
lpd-5
K
dct-1::GFP
Relative fluorescence
0
1
2
3
4
5
****
***
con
nuo-5
lpd-5
L
hlh-30::GFP
% of animals wit nuclear localization of HLH-30::GFP
0
20
40
60
80
****
****
con
nuo-5
lpd-5

Figure 3

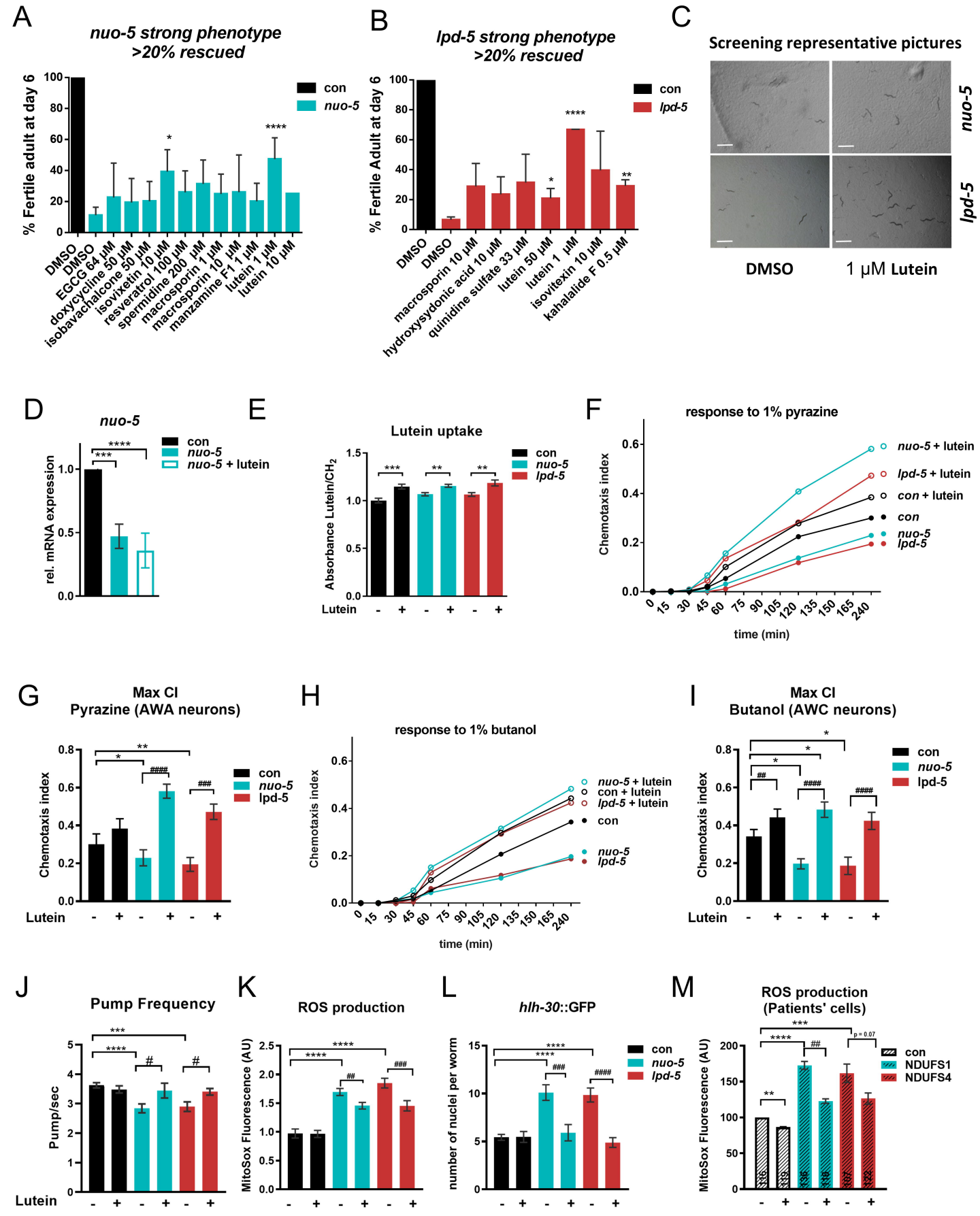
A
nuo-5 strong phenotype
>20% rescued
% Fertile adult at day 6
con
nuo-5
DMSO
DMSO
EGCG 64 µM
doxycycline 50 µM
isobavachalcone 50 µM
isovitexin 10 µM
resveratrol 100 µM
spermidine 200 µM
macrosporin 1 µM
macrosporin 10 µM
manzamine F1 1 µM
lutein 1 µM
lutein 10 µM
B
lpd-5 strong phenotype
>20% rescued
% Fertile Adult at day 6
con
lpd-5
DMSO
DMSO
macrosporin 10 µM
hydroxysydonic acid 10 µM
quinidine sulfate 33 µM
lutein 50 µM
lutein 1 µM
isovitexin 10 µM
kahalalide F 0.5 µM
C
Screening representative pictures
nuo-5
lpd-5
DMSO
1 µM Lutein
D
nuo-5
rel. mRNA expression
con
nuo-5
nuo-5 + lutein
E
Lutein uptake
Absorbance Lutein/CH2
con
nuo-5
lpd-5
Lutein
F
response to 1% pyrazine
Chemotaxis index
nuo-5 + lutein
lpd-5 + lutein
con + lutein
con
nuo-5
lpd-5
time (min)
G
Max CI
Pyrazine (AWA neurons)
Chemotaxis index
con
nuo-5
lpd-5
Lutein
H
response to 1% butanol
Chemotaxis index
nuo-5 + lutein
con + lutein
lpd-5 + lutein
con
nuo-5
lpd-5
time (min)
I
Max CI
Butanol (AWC neurons)
Chemotaxis index
con
nuo-5
lpd-5
Lutein
J
Pump Frequency
Pump/sec
Lutein
K
ROS production
MitoSox Fluorescence (AU)
L
hlh-30::GFP
number of nuclei per worm
con
nuo-5
lpd-5
M
ROS production
(Patients' cells)
MitoSox Fluorescence (AU)
p = 0.07
con
NDUFS1
NDUFS4

Figure 4

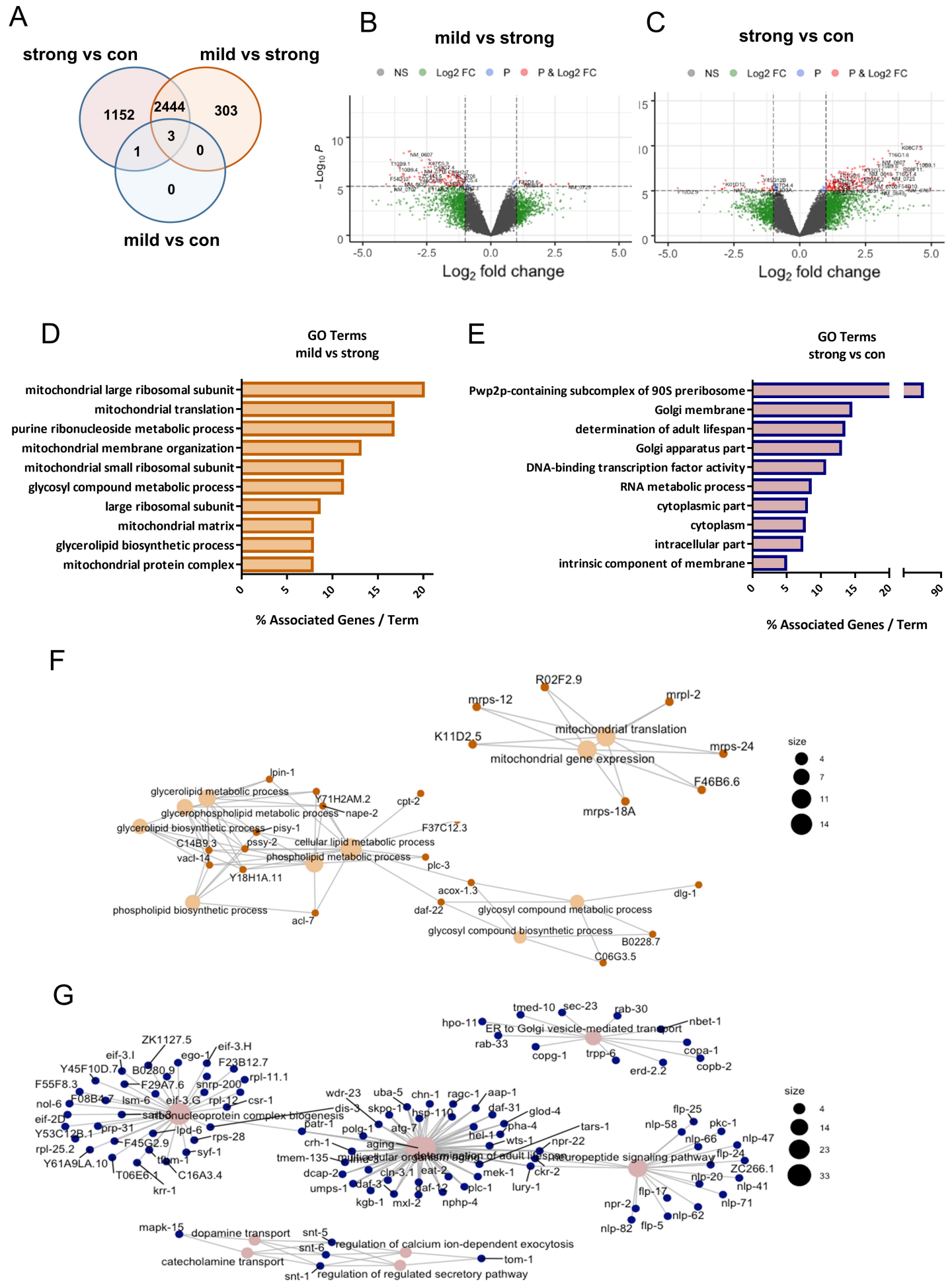
A
strong vs con
mild vs strong
mild vs con
1152
2444
303
3
1
0
0
B
mild vs strong
NS
Log2 FC
P
P & Log2 FC
−Log10 P
Log2 fold change
C
strong vs con
NS
Log2 FC
P
P & Log2 FC
Log2 fold change
D
GO Terms
mild vs strong
mitochondrial large ribosomal subunit
mitochondrial translation
purine ribonucleoside metabolic process
mitochondrial membrane organization
mitochondrial small ribosomal subunit
glycosyl compound metabolic process
large ribosomal subunit
mitochondrial matrix
glycerolipid biosynthetic process
mitochondrial protein complex
% Associated Genes / Term
E
GO Terms
strong vs con
Pwp2p-containing subcomplex of 90S preribosome
Golgi membrane
determination of adult lifespan
Golgi apparatus part
DNA-binding transcription factor activity
RNA metabolic process
cytoplasmic part
cytoplasm
intracellular part
intrinsic component of membrane
% Associated Genes / Term
F
R02F2.9
mrps-12
mrpl-2
K11D2.5
mitochondrial translation
mitochondrial gene expression
mrps-24
F46B6.6
mrps-18A
size
lpin-1
glycerolipid metabolic process
Y71H2AM.2
cpt-2
glycerophospholipid metabolic process
nape-2
glycerolipid biosynthetic process
pisy-1
F37C12.3
C14B9.3
pssy-2
cellular lipid metabolic process
vacl-14
phospholipid metabolic process
plc-3
Y18H1A.11
acox-1.3
dlg-1
phospholipid biosynthetic process
acl-7
daf-22
glycosyl compound metabolic process
glycosyl compound biosynthetic process
B0228.7
C06G3.5
G
tmed-10
sec-23
rab-30
hpo-11
nbet-1
ER to Golgi vesicle-mediated transport
rab-33
copg-1
trpp-6
copa-1
erd-2.2
copb-2
ZK1127.5
eif-3.H
eif-3.I
ego-1
F23B12.7
Y45F10D.7
B0280.9
rpl-11.1
F55F8.3
F29A7.6
snrp-200
nol-6
F08B4.7
lsm-6
eif-3.G
rpl-12
csr-1
eif-2D
satb
nucleoprotein complex biogenesis
Y53C12B.1
prp-31
lpd-6
rps-28
rpl-25.2
F45G2.9
syf-1
Y61A9LA.10
tfam-1
T06E6.1
C16A3.4
krr-1
wdr-23
uba-5
chn-1
ragc-1
aap-1
dis-3
skpo-1
hsp-110
daf-31
glod-4
patr-1
polg-1
atg-7
pha-4
tars-1
hel-1
wts-1
npr-22
crh-1
aging
tmem-135
determination of adult lifespan
neuropeptide signaling pathway
dcap-2
cln-3.1
eat-2
mek-1
ckr-2
umps-1
daf-3
daf-12
plc-1
lury-1
kgb-1
mxl-2
nphp-4
flp-25
nlp-58
pkc-1
nlp-66
nlp-47
flp-24
ZC266.1
nlp-20
nlp-41
flp-17
nlp-71
npr-2
nlp-62
nlp-82
flp-5
size
mapk-15
dopamine transport
snt-5
snt-6
regulation of calcium ion-dependent exocytosis
catecholamine transport
tom-1
snt-1
regulation of regulated secretory pathway

Figure 5

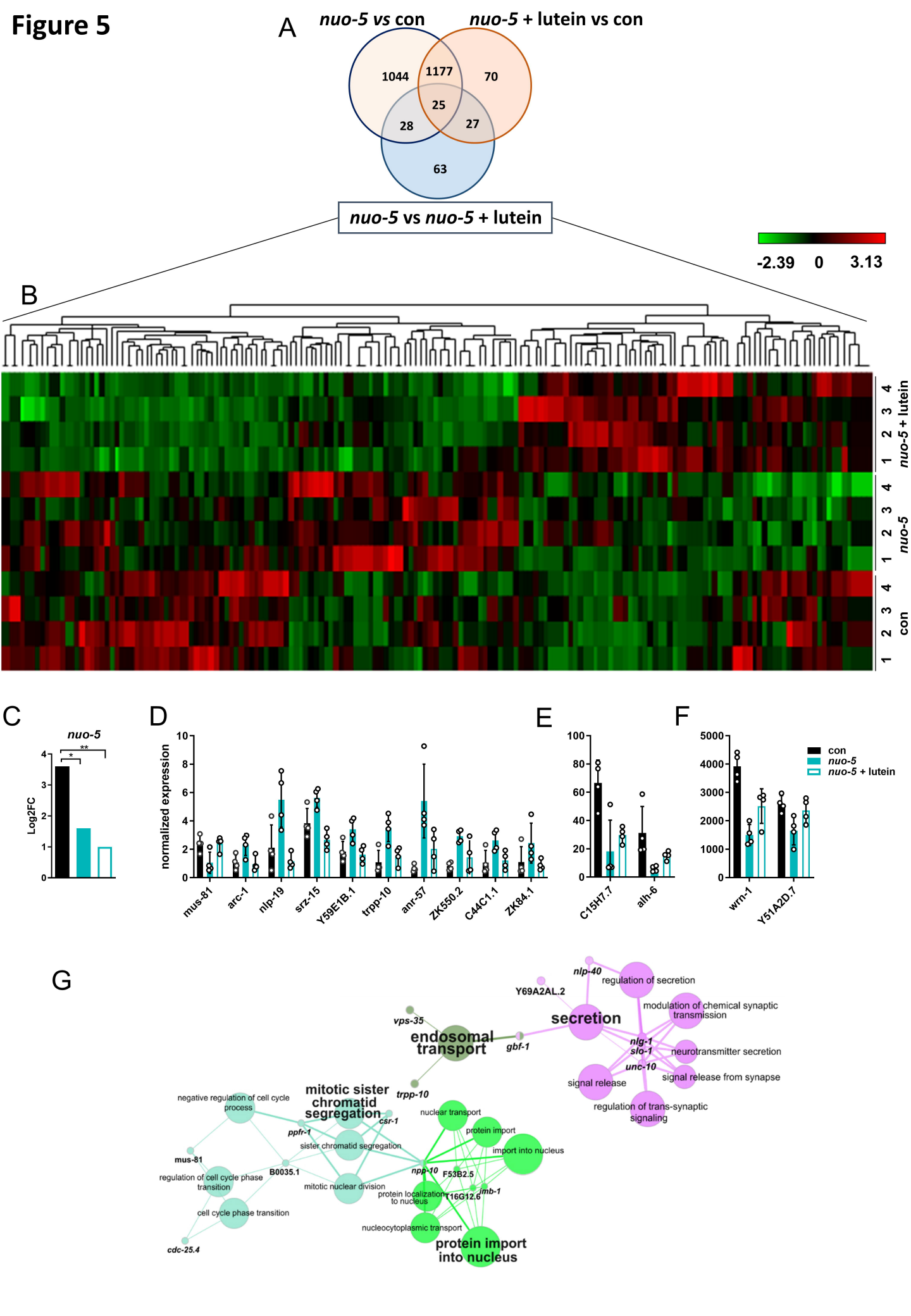
A
nuo-5 vs con
nuo-5 + lutein vs con
1044
1177
70
25
28
27
63
nuo-5 vs nuo-5 + lutein
-2.39
0
3.13
B
nuo-5 + lutein
nuo-5
con
C
nuo-5
Log2FC
D
normalized expression
mus-81
arc-1
nlp-19
srz-15
Y59E1B.1
trpp-10
anr-57
ZK550.2
C44C1.1
ZK84.1
E
C15H7.7
aln-6
F
wrn-1
Y51A2D.7
con
nuo-5
nuo-5 + lutein
G
nlp-40
regulation of secretion
Y69A2AL.2
modulation of chemical synaptic transmission
secretion
vps-35
endosomal transport
gbf-1
nlg-1
slo-1
neurotransmitter secretion
unc-10
signal release from synapse
signal release
regulation of trans-synaptic signaling
trpp-10
mitotic sister chromatid segregation
negative regulation of cell cycle process
csr-1
ppfr-1
sister chromatid segregation
nuclear transport
protein import
import into nucleus
mus-81
B0035.1
regulation of cell cycle phase transition
mitotic nuclear division
npp-10
F53B2.5
protein localization to nucleus
T16G12.6
jmb-1
cell cycle phase transition
nucleocytoplasmic transport
cdc-25.4
protein import into nucleus

Figure 6

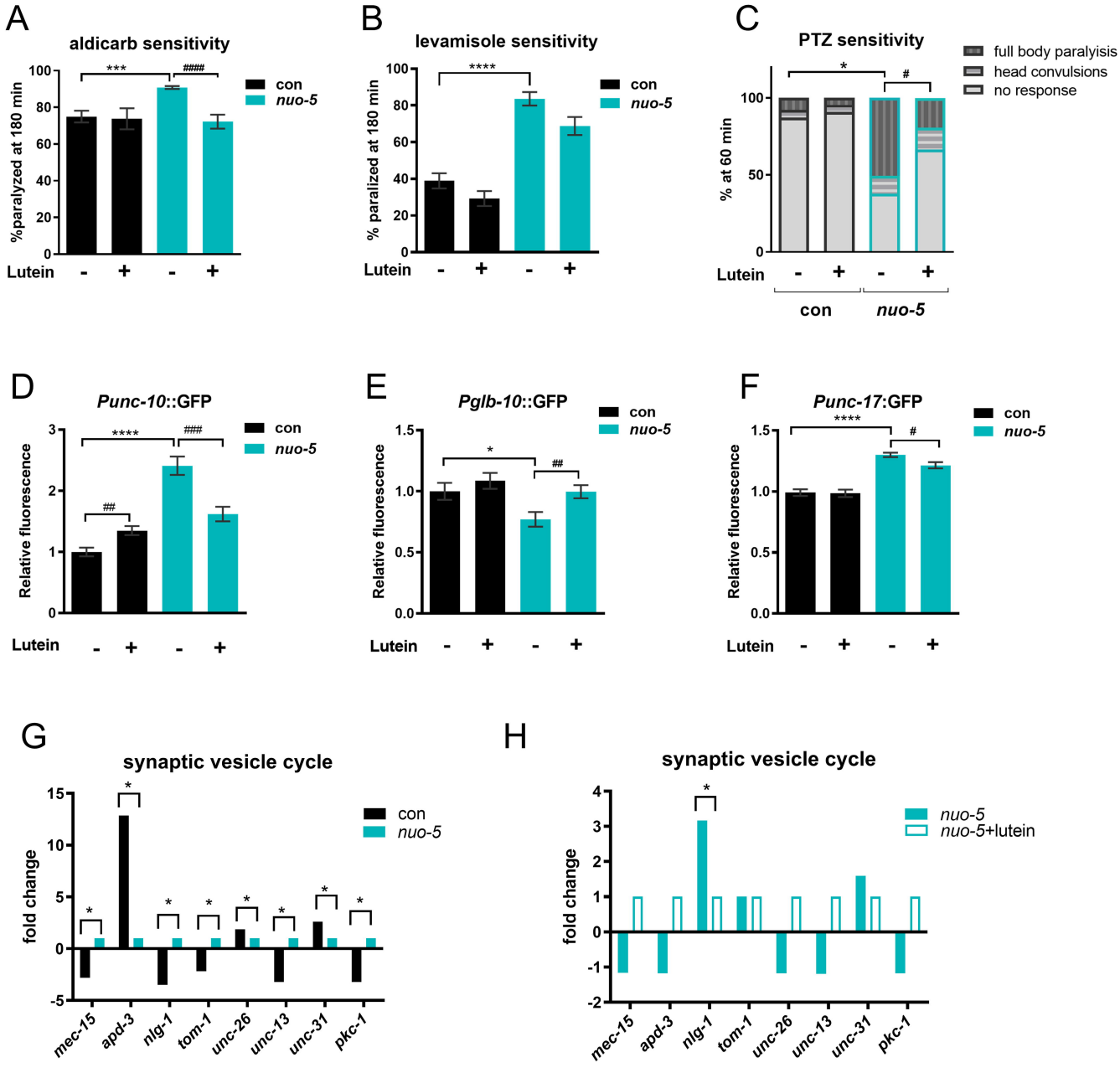
A
aldicarb sensitivity
%paralyzed at 180 min
con
nuo-5
Lutein
B
levamisole sensitivity
% paralized at 180 min
C
PTZ sensitivity
% at 60 min
full body paralyisis
head convulsions
no response
D
Punc-10::GFP
Relative fluorescence
E
Pglb-10::GFP
F
Punc-17:GFP
G
synaptic vesicle cycle
fold change
mec-15
apd-3
nlg-1
tom-1
unc-26
unc-13
unc-31
pkc-1
H
nuo-5
nuo-5+lutein

Figure 7

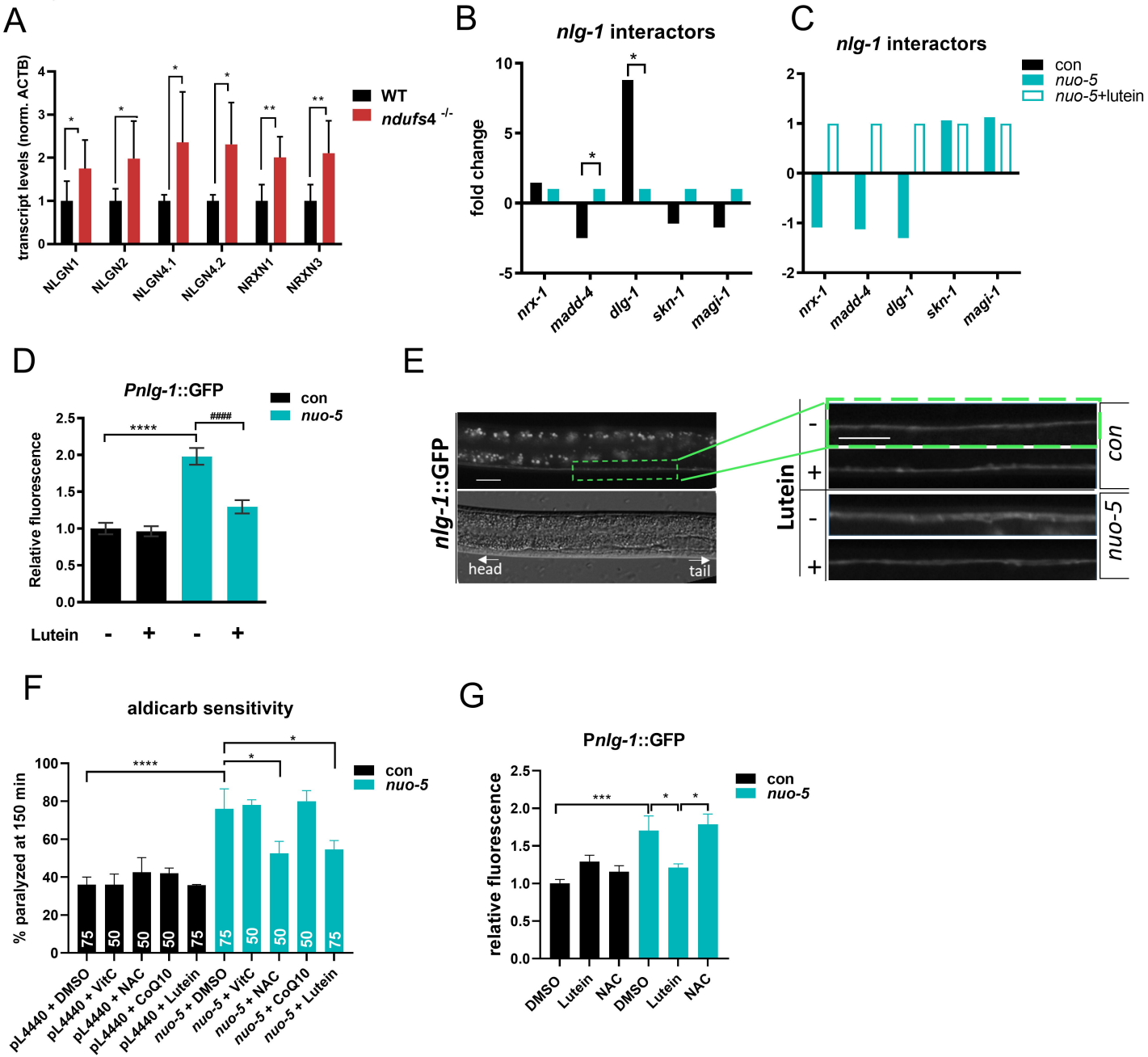
A
transcript levels (norm. ACTB)
WT
ndufs4 -/-
NLGN1
NLGN2
NLGN4.1
NLGN4.2
NRXN1
NRXN3
B
nlg-1 interactors
fold change
nrx-1
madd-4
dlg-1
skn-1
magl-1
C
nlg-1 interactors
con
nuo-5
nuo-5+lutein
D
Pnlg-1::GFP
Relative fluorescence
Lutein
E
nlg-1::GFP
head
tail
Lutein
con
nuo-5
F
aldicarb sensitivity
% paralyzed at 150 min
pL4440 + DMSO
pL4440 + VitC
pL4440 + NAC
pL4440 + CoQ10
pL4440 + Lutein
nuo-5 + DMSO
nuo-5 + VitC
nuo-5 + NAC
nuo-5 + CoQ10
nuo-5 + Lutein
G
Pnlg-1::GFP
relative fluorescence
DMSO
Lutein
NAC

Figure 8

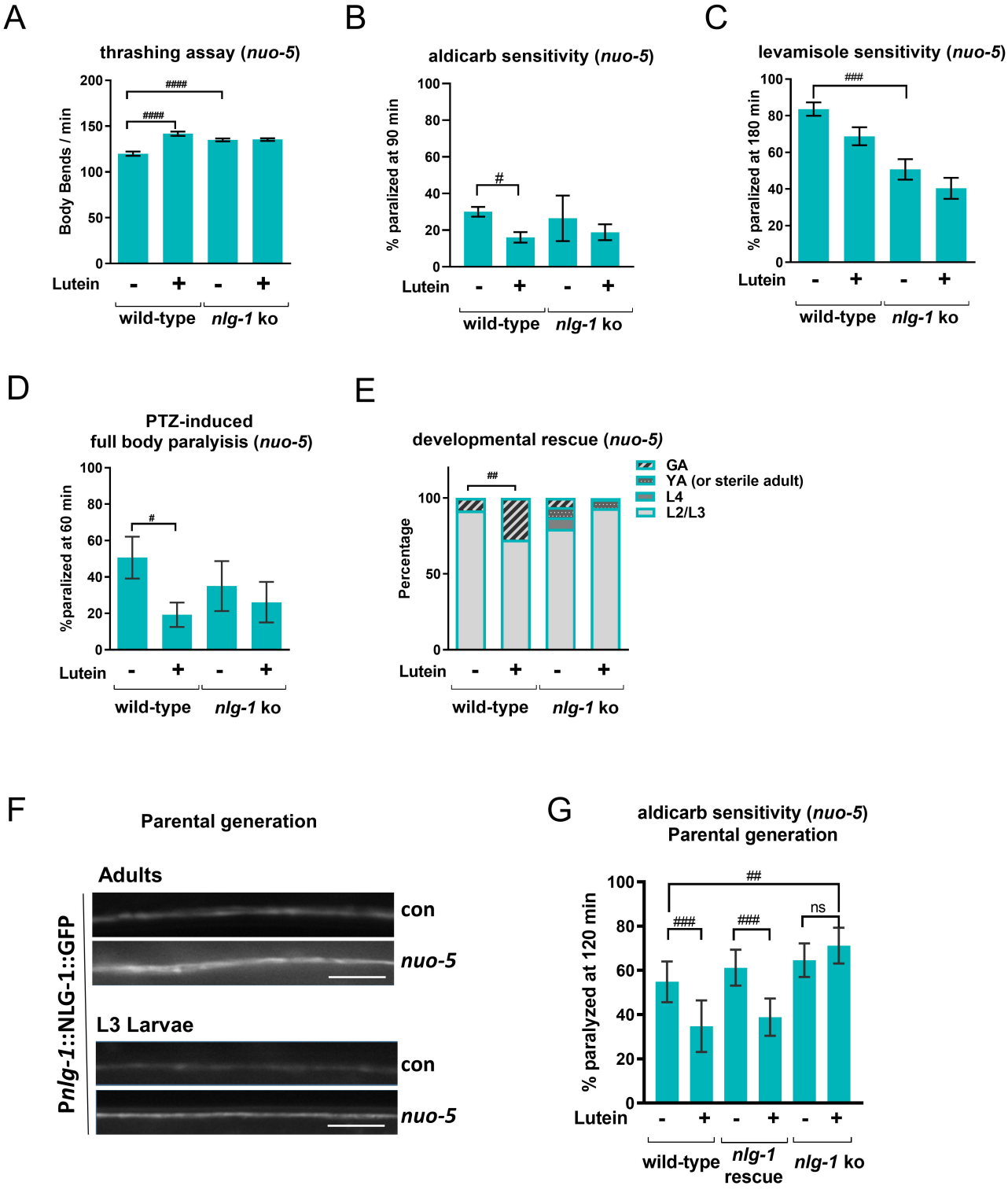
A
thrashing assay (nuo-5)
Body Bends / min
200
150
100
50
0
####
####
Lutein
-
+
-
+
wild-type
nlg-1 ko
B
aldicarb sensitivity (nuo-5)
% paralized at 90 min
100
80
60
40
20
0
#
Lutein
-
+
-
+
wild-type
nlg-1 ko
C
levamisole sensitivity (nuo-5)
% paralized at 180 min
100
80
60
40
20
0
###
Lutein
-
+
-
+
wild-type
nlg-1 ko
D
PTZ-induced
full body paralyisis (nuo-5)
%paralized at 60 min
100
80
60
40
20
0
#
Lutein
-
+
-
+
wild-type
nlg-1 ko
E
developmental rescue (nuo-5)
Percentage
100
50
0
##
GA
YA (or sterile adult)
L4
L2/L3
Lutein
-
+
-
+
wild-type
nlg-1 ko
F
Parental generation
Adults
con
nuo-5
L3 Larvae
con
nuo-5
Pnlg-1::NLG-1::GFP
G
aldicarb sensitivity (nuo-5)
Parental generation
% paralyzed at 120 min
100
80
60
40
20
0
##
###
###
ns
Lutein
-
+
-
+
-
+
wild-type
nlg-1
rescue
nlg-1 ko